Glacial onset predated Late Ordovician climate cooling

Alexandre Pohl, Yannick Donnadieu, Guillaume Le Hir, Jean-baptiste Ladant, Christophe Dumas, Jorge Alvarez-solas, Thijs Vandenbroucke

AGU PUBLICATIONS

Paleoceanography

RESEARCH ARTICLE
10.1002/2016PA002928

Glacial onset predated Late Ordovician climate cooling

Alexandre Pohl[1], Yannick Donnadieu[1], Guillaume Le Hir[2], Jean-Baptiste Ladant[1], Christophe Dumas[1], Jorge Alvarez-Solas[3], and Thijs R. A. Vandenbroucke[4,5]

[1]Laboratoire des Sciences du Climat et de l'Environnement, LSCE/IPSL, CEA-CNRS-UVSQ, Université Paris-Saclay, Gif-sur-Yvette, France, [2]Institut de Physique du Globe de Paris, Université Paris7-Denis Diderot, 1 rue Jussieu, Paris, France, [3]Departamento Astrofísica y Ciencias de la Atmósfera, Universidad Complutense de Madrid, Madrid, Spain, [4]Department of Geology, Ghent University, Krijgslaan, Belgium, [5]Evo-Eco-Paléo UMR 8198, Université de Lille, Villeneuve d'Ascq CEDEX, France

Abstract The Ordovician glaciation represents the acme of one of only three major icehouse periods in Earth's Phanerozoic history and is notorious for setting the scene for one of the "big five" mass extinction events. Nevertheless, the mechanisms that drove ice sheet growth remain poorly understood and the final extent of the ice sheet crudely constrained. Here using an Earth system model with an innovative coupling method between ocean, atmosphere, and land ice accounting for climate and ice sheet feedback processes, we report simulations portraying for the first time the detailed evolution of the Ordovician ice sheet. We show that the emergence of the ice sheet happened in two discrete phases. In a counterintuitive sequence of events, the continental ice sheet appeared suddenly in a warm climate. Only during the second act, and set against a background of decreasing atmospheric CO_2, followed steeply dropping temperatures and extending sea ice. The comparison with abundant sedimentological, geochemical, and micropaleontological data suggests that glacial onset may have occurred as early as the Middle Ordovician Darriwilian, in agreement with recent studies reporting third-order glacioeustatic cycles during the same period. The second step in ice sheet growth, typified by a sudden drop in tropical sea surface temperatures by ~8°C and the further extension of a single, continental-scale ice sheet over Gondwana, marked the onset of the Hirnantian glacial maximum. By suggesting the presence of an ice sheet over Gondwana throughout most of the Middle and Late Ordovician, our models embrace the emerging paradigm of an "early Paleozoic Ice Age."

Key Points:
- Earth system model providing the first detailed simulation of Middle to Late Ordovician land ice growth
- Model/data comparison suggests a Darriwilian age for glacial onset
- A single ice sheet of large extent covered Gondwana during the Hirnantian glacial maximum

Supporting Information:
- Supporting Information S1
- Supporting Information S2
- Figure S1

Correspondence to:
A. Pohl,
pohl.alexandre@gmail.com

Citation:
Pohl, A., Y. Donnadieu, G. Le Hir, J.-B. Ladant, C. Dumas, J. Alvarez-Solas, and T. R. A.Vandenbroucke (2016), Glacial onset predated Late Ordovician climate cooling, *Paleoceanography*, *31*, 800–821, doi:10.1002/2016PA002928.

Received 20 JAN 2016
Accepted 21 MAY 2016
Accepted article online 28 MAY 2016
Published online 25 JUN 2016

1. Introduction

The Middle to Late Ordovician (470–444 Ma) has long been considered an enigmatic and unique period in Earth's history. Much of this mystery revolved around our inability to explain how a glacial pulse [*Finnegan et al.*, 2011], high pCO_2 levels potentially exceeding 20 times the preindustrial atmospheric level [*Berner*, 1990; *Yapp and Poths*, 1996] (PAL, 1 PAL = 280 ppm), a global biodiversity crisis [*Sheehan*, 2001], and major perturbations of the carbon cycle [*Brenchley et al.*, 1994] could have coincided. Over the last few years, however, evidence has accumulated that some of these apparent conflicts may have resulted from erroneous interpretations of the relatively poorly preserved and incomplete Ordovician sedimentary record [*Ghienne et al.*, 2014]. Recent studies suggest that the atmospheric CO_2 content was probably much lower than had been previously proposed [*Rothman*, 2002; *Herrmann et al.*, 2004; *Berner*, 2006; *Vandenbroucke et al.*, 2010a; *Pancost et al.*, 2013] and that ocean temperatures reached modern-like values as early as the Middle Ordovician, distinctly contrasting with earlier visions of a perennial Ordovician supergreenhouse [*Trotter et al.*, 2008; *Vandenbroucke et al.*, 2009]. Despite a more comprehensive analysis of the physical evidence, major uncertainties persist about the mechanisms that drove ice sheet growth and about its final extent. Rooted in the disperse nature of the Late Ordovician glacial sedimentary records in North Africa [*Ghienne et al.*, 2007], South Africa, and South America [*Díaz-Martínez and Grahn*, 2007], one of the major questions remains whether those glacial outcrops are indicative of a single, large ice sheet that developed from North Africa (then at a polar latitude) to South Africa (at tropical latitudes in latest reconstructions) [*Torsvik and Cocks*, 2013] or if independent ice sheets of smaller extent coexisted over the South Pole and in the tropics [*Ghienne et al.*, 2007; *Le Heron and Dowdeswell*, 2009].

It is also still unclear how glacial onset could have possibly occurred in the midst of a prolonged period of hot climate. Evidence for warm shallow seas in the tropics (up to 37°C) [*Finnegan et al.*, 2011], as suggested by most recent Ordovician geochemical data [*Trotter et al.*, 2008; *Finnegan et al.*, 2011], is in apparent contradiction with Middle to Upper Ordovician deposits where glacioeustatic events are identified [*Loi et al.*, 2010; *Turner et al.*, 2012; *Elrick et al.*, 2013; *Dabard et al.*, 2015; *Rasmussen et al.*, 2016] or suggested [*Nielsen*, 2004] (see discussion in *Amberg et al.* [2016]). These eustatic cycles support the presence of ice sheets since the Middle Ordovician Darriwilian (467 Ma) rather than a sudden emplacement of a massive ice sheet restricted to the Hirnantian stage (445–444 Ma).

To investigate how these apparently contradictive interpretations can be reconciled, we employ an Earth system model to propose the first realistic simulations of Middle to Late Ordovician ice sheet growth. The last modeling attempts of this kind date back to two papers published by *Herrmann et al.* [2003, 2004]. Building on the seminal studies of *Crowley and Baum* [1991, 1995], they provided major insights into the climatic conditions required to trigger Late Ordovician glacial onset. However, they are more than 10 years old, and the experimental setup that is available to us has significantly advanced. *Herrmann et al.*'s [2003, 2004] models notably did not resolve ice sheet feedbacks on global climate. The simulated ice sheet did not extend beyond 60°S and therefore poorly compared to the Ordovician glacial sedimentary record [e.g., *Ghienne et al.*, 2007]. More recently, *Lowry et al.* [2014] asynchronously coupled a slab mixed-layer ocean-atmosphere general circulation model (GENESIS) with an ice sheet model to investigate the impact of the changes in continental configuration on the potential for glacial inception throughout the Paleozoic. However, they did not use specific Ordovician boundary conditions in their coupled simulations—in terms of topography, solar luminosity, and CO_2 level in particular—which resulted in significant discrepancies between Ordovician geological data and modeled ice sheet extent and flow. The flat topography led to an unexpected ice sheet geometry with the maximum ice sheet height simulated along the coasts of Gondwana at 440 Ma. The resulting ice sheet flowed from the coast to the continent interior (*Lowry et al.* [2014]; see their discussion section), at odds with the sedimentary record of the Hirnantian glaciation [e.g., *Ghienne et al.*, 2007]. They ran additional experiments considering the evolution of the solar luminosity value throughout the Paleozoic, but they did not account for the feedbacks of the ice sheet on global climate in these simulations. To capture processes leading to glacial onset and ensure both reliable ice sheet growth mechanisms and robust steady state ice sheet extent, we here use suitable boundary conditions together with an innovative modeling procedure that for the first time in the Ordovician considers ocean-atmosphere-ice sheet interplays as well as a fully dynamic ocean component. Our model accounts for Ordovician orbital variations and for the wide range of suggested CO_2 levels, i.e., 3–24 PAL (see section 2.2.2).

We compare our modeling results with abundant geochemical, sedimentological, and paleontological data, which provides additional insights into both the extent and duration of the glaciation. However, current ice sheet models exhibit severe issues of hysteresis, making land ice too stable and requiring unreasonably high atmospheric CO_2 levels to cause continental-scale ice sheet retreats [*Pollard and DeConto*, 2005; *Horton and Poulsen*, 2009]. Therefore, we did not attempt the simulation of the Late Ordovician deglaciation but identify this as a target for the future. We are confident that ongoing advances in modeling of the cryosphere [*Ganopolski et al.*, 2010; *Pollard et al.*, 2015; *Gasson et al.*, 2016] will help resolve this issue in the years to come.

2. Methods

2.1. Asynchronous Coupling Design

The deep-time Earth system model used throughout the study is described below. Our aim is to simulate ice sheet-climate equilibria under decreasing pCO_2, representative of the well-established Ordovician cooling trend [*Trotter et al.*, 2008]. This requires coupling an ocean-atmosphere general circulation model with an ice sheet model. The most straightforward way to couple an ocean-atmosphere climate model to an ice sheet model is the purely synchronous coupling method, which would account for exchanges between the ocean, atmosphere, and land ice components at each model time step. The long computational time required by an ocean-atmosphere general circulation model (GCM), however, forbids the use of synchronous coupling to solve deep-time issues, which usually require long ice sheet runs lasting hundreds of thousands of model years [e.g., *Ladant et al.*, 2014]. Several alternative methods have therefore been proposed [*Pollard*, 2010], including asynchronous coupling with a GCM lookup table, which remains the only solution applicable on very long

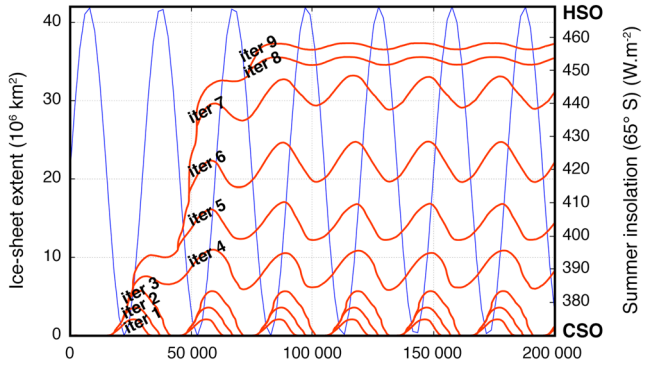

Figure 1. Ice sheet results obtained at 12 PAL, with our Earth system model accounting for orbital variations and ice sheet feedbacks on climate, throughout the successive asynchronous coupling steps. Red curves represent the evolution of the land ice cover through ice sheet model integration time (200 kyr per iteration). The thin blue line stands for the 30 kyr obliquity forcing used to interpolate between the CSO and the HSO. The associated right *y* axis gives the Southern Hemisphere mean summer insolation received at 65°S. The ice sheet model (GRISLI) is first run for 200 kyr from its initial, ice-free state (iter 1), by linearly interpolating between the CSO and HSO temperature and precipitation forcing fields according to the 30 kyr Ordovician obliquity period. Then, the largest ice sheet simulated during this first iteration is returned as a boundary condition to the climate models. New climatic forcing fields are simulated, which therefore take the ice-albedo local radiative effect into account. The latter climatic snapshots are added to the "ice cover" dimension of the GCM lookup table, providing new climatic fields to interpolate with. GRISLI is once again run for 200 kyr from its ice-free state (iter 2), and the ice sheet model climatic forcing fields are interpolated as a function of time both between the CSO and the HSO and between the ice-free state and the glaciated state predicted from previous iteration. The largest ice sheet simulated is used to force the third iteration (new climatic snapshots are added to the GCM lookup table), and the loop is repeated until the ice sheet is in equilibrium with global climate (iter 4 to iter 9), i.e., an additional iteration does not induce a much larger ice sheet extent (compare iter 8 and iter 9).

time scales [e.g., *Ladant et al.*, 2014]. In this method, GCM snapshots are gathered into a multidimensional matrix. Each dimension of the matrix corresponds to a given external forcing (e.g., the orbital configuration or the pCO_2) and contains surface temperature and precipitation fields simulated for several values of this forcing, which provide the entire information required during the subsequent ice sheet model integration. Then, at any point in the long-term ice sheet model run, the surface mass balance of the ice sheet is calculated based on mean monthly temperature and precipitation fields interpolated between the appropriate cells of the matrix [*Pollard*, 2010]. In the present case study, the GCM snapshots are collected in a matrix with three dimensions, i.e., the Earth's orbital parameters, the ice sheet size, and the pCO_2, following the methodology successfully applied to the Antarctic ice sheet onset at the Eocene-Oligocene transition [*Ladant et al.*, 2014]. However, unlike the Antarctic ice sheet, which has limited spatial extent, the maximum ice sheet extent over the vast Gondwana paleocontinent is virtually unlimited, and as such, there is no reason to preconceive any maximum ice sheet extent prior to the buildup of the 3-D matrix. Here the ice sheet sizes are not prescribed, hence evolving freely, instead of imposing successive ice sheet extents for the interpolation. As a consequence we build the matrix step by step.

1. Climatic snapshots representative of ice-free conditions are first obtained: for a given pCO_2 (first dimension of the matrix), two climate states are computed by the GCM with an ice-free bedrock topography (second dimension), for two opposed orbital configurations (third dimension) yielding either a cold or a warm summer over the southern high latitudes (cold and hot summer orbits—CSO and HSO, respectively—see section 2.2.2).
2. A first ice sheet is modeled: the ice sheet model is run, for the same pCO_2 level, using a sinusoidal forcing in obliquity weighted between the two opposite climates from step 1 (iter 1 in Figure 1). The period of the sinusoidal variation in obliquity is set to 30 kyr, based on spectral analysis of Ordovician halite deposits [*Williams*, 1991]. Orbital variations are known as a major driver of Pleistocene glacial cycles [e.g., *Paillard*, 1998], and they have been shown to significantly impact the growth of the ice sheet during the Ordovician as well [*Herrmann et al.*, 2003; *Ghienne et al.*, 2014; *Dabard et al.*, 2015].
3. An ice sheet of larger extent is simulated, provided that climate is favorable to ice sheet growth: in order to account for the feedbacks of the ice sheet on climate, the largest ice sheet simulated previously is reintroduced as a boundary condition into the climate model (still keeping the CO_2 constant). Two additional glacial climatic states are simulated, one for each of the two opposite orbital configurations (CSO and HSO). The climatic snapshots are gathered into the matrix of climatic states, each snapshot corresponding to a specific land ice mask and orbital configuration (i.e., a CSO snapshot and a HSO snapshot for each ice sheet extent, including the ice-free state). The ice sheet model is then run, starting from an ice-free state, forced in temperature and precipitation using climatic fields interpolated, throughout model integration time,

between the climatic snapshots of the matrix as a function of both the orbital forcing and the extent of the ice sheet (iter 2 in Figure 1).

4. Step 3 is repeated until steady state is reached between land ice and global climate: a new member is thus added to the "ice sheet extent" dimension of the matrix as many times as necessary, and the resulting ice sheet is neither limited to a given geometry nor artificially pulled toward a maximal extent, which might have been the case with prescribed ice sheets (iter 3 to iter 9 in Figure 1).
5. The whole procedure is repeated for the other CO_2 values.

Climatic snapshots are obtained using successively the ocean-atmosphere general circulation model FOAM (as a sea surface temperature generator) and the state-of-the-art atmospheric model LMDZ, with the same boundary conditions. The model FOAM is first integrated until deep-ocean equilibrium is reached (≥2000 years). Given that the atmospheric fields of temperature and precipitation simulated with FOAM are not sufficiently well resolved to directly force the ice sheet model GRISLI, the sea surface temperatures simulated with FOAM are subsequently used to force the atmospheric model LMDZ, the outputs of which are in turn used to force GRISLI. The alternate use of FOAM and LMDZ has been shown to perform well, as testified by previously published paleoclimate studies [*Ladant et al.*, 2014; *Licht et al.*, 2014].

2.2. Model Setup

2.2.1. Model Details

FOAM (Fast Ocean Atmosphere Model) version 1.5 is a fully coupled mixed-resolution ocean-atmosphere general circulation model with no flux corrections [*Jacob*, 1997]. Its quick turnaround time allows for long millennium-scale integrations. FOAM is consequently well designed for paleoclimate studies, for which purpose it has been routinely used in the past, including for the Ordovician [*Nardin et al.*, 2011; *Pohl et al.*, 2014, 2015]. The atmospheric component of the model is the National Center for Atmospheric Research's (NCAR) Community Climate Model version 2 (CCM2) benefitting from the upgraded radiative and hydrologic physics from CCM3 version 3.2. It is run at a R15 spectral resolution (4.5° × 7.5°) with 18 vertical levels (14 in the troposphere). The ocean module is the Ocean Model version 3 (OM3). It is a finite difference, 24-level *z* coordinate ocean general circulation model providing a higher resolution than the atmospheric module (1.4° × 2.8°) on a rectangular grid. Sea ice is simulated using the thermodynamics of the NCAR's Climate System Model 1.4 sea ice module, which is based on the *Semtner* [1976] three-layer thermodynamic snow/ice model.

The LMDZ (Laboratoire de Météorologie Dynamique Zoom) model is an IPCC-class (Intergovernmental Panel on Climate Change) atmospheric general circulation model benefitting, as the atmospheric component of the state-of-the-art IPSL (Institut Pierre-Simon Laplace) Earth system model, from the latest physical and dynamical refinements [*Hourdin et al.*, 2013]. A midresolution version of the model is used in this study, providing a resolution of 1.9° × 3.75° with 39 vertical levels (21 in the troposphere) on a rectangular grid.

GRISLI (GRenoble Ice-Shelf and Land Ice) is a three-dimensional ice sheet model accounting for thermodynamical coupling between ice velocities and temperatures [*Ritz et al.*, 2001]. GRISLI runs at 40 km × 40 km resolution and simulates both grounded and floating ice, by considering three types of ice flow: ice sheets, ice streams, and ice shelves. At each time step, the model determines the areas where each type of ice flow applies. Ice shelves are large floating ice plates fed by inland ice. Their location is determined based on a flotation criterion, and ice velocities in these grid points are computed using the shallow-shelf approximation with a basal stress set to zero. The FOAM model does not have the resolution needed to simulate oceanic melting under the ice shelves. This requires specific experimental setups, involving high-resolution (regional) climate models accounting for ocean temperature and circulation patterns under the shelves [e.g., *Heimbach and Losch*, 2012]. In this study, we therefore used a parameterization considering a basic dependence of the melt rate on the ocean bathymetry. We imposed a melt rate of 0.2 m yr^{-1} on the continental shelf (water depth ≤600 m) and 2 m yr^{-1} in open ocean conditions (water depth >600 m). These values are well within the range defined in previous studies on Antarctica [*Pollard and DeConto*, 2012, their Figure 4b]. Calving occurs when the thickness of the ice shelf drops below 150 m. All areas that are not ice shelves are grounded ice, including ice sheets and ice stream zones. Ice sheets are regions of grounded ice where ice flow is mainly due to deformation, basal sliding occurring only where the base is at the pressure melting point. Inland ice velocity fields are computed using the shallow-ice approximation. Because the latter is inaccurate to simulate fast-flowing ice [*Bueler and Brown*, 2009], such regions—the ice stream zones—are specifically treated by the model. Ice streams are corridors of fast flow with widths of a few kilometers, usually smaller than the

model grid size. It is not possible to simulate them individually. Their effect is parameterized in the model by treating areas which have the large-scale characteristics of ice streams independently. Ice stream zones are defined based on both the local slope of the terrain and the effective water pressure below the ice sheet, the latter as a function of the subglacial water depth. Ice flow in these ice stream zones is computed using both the shallow-ice and the shallow-shelf approximations. Contrary to what is prescribed for ice shelves, basal stress is not set to zero. GRISLI simulates the evolution of ice sheets in response to climatic forcing. The model calculates the surface mass balance of the ice sheet as the sum of accumulation minus ablation, using mean monthly surface temperature and precipitation. Ablation is in turn computed with the positive degree day (PDD) method, using a surface melt refreezing rate of 60% and a standard deviation (σ) of 5°C to represent the air temperature variability over the month [*Reeh*, 1991]. The PDD model is based on an empirical relation between air temperature and melting rate, assuming that the near-surface temperature transmits the majority of the climatic forcing to the ice sheet. Despite its simplicity, this ablation scheme has been shown to perform well [e.g., *Ladant et al.*, 2014], although some recent studies suggest that explicitly accounting for the melt contribution from insolation may significantly impact the calculation of surface melt [e.g., *Robinson and Goelzer*, 2014]. GRISLI also accounts for the isostatic adjustment of the bedrock in response to ice load. The common "elastic lithosphere/relaxing asthenosphere" (ELRA) model is used. In this parameterization, the bed underneath the ice sheet is described as a thin, elastic lithosphere governing the spatial shape of the deflection by allowing a regional response to the ice load. The underlying, viscous asthenosphere governs the time-dependent characteristics of the deformation through a standard relaxation time of 3 kyr. GRISLI was initially developed for and validated over Antarctica by *Ritz et al.* [2001]. It has since then been successfully applied to study the mechanisms that drove Heinrich events (last 80 ka) [*Alvarez-Solas et al.*, 2011, 2013], the inception of the Fennoscandian ice sheet during the last glacial period (90 ka) [*Peyaud et al.*, 2007], the partial melt of the Greenland ice sheet during the last interglacial period (130–115 ka) [*Quiquet et al.*, 2013], and the continental-scale initiation of the Antarctic ice sheet at the Eocene-Oligocene boundary (34 Ma) [*Ladant et al.*, 2014].

2.2.2. Boundary Conditions

We use the Late Ordovician (450 Ma) continental configuration from *Blakey* [2016]. Given that continental vegetation was restricted to nonvascular plants during the Ordovician [*Steemans et al.*, 2009; *Rubinstein et al.*, 2010]—the coverage of which is difficult to estimate—we follow previous studies about Ordovician climate [*Nardin et al.*, 2011; *Pohl et al.*, 2014, 2015] in imposing a bare soil (rocky desert) on every continental grid point. Five realistic topographic classes are used, ranging from the deep ocean (−4000 m) to the Caledonian orogen (3000 m) [*Pohl et al.*, 2014]. Simulations are conducted for two end-member orbital configurations (CSO and HSO), respectively, extremely favorable and unfavorable to south polar ice sheet growth. The HSO (CSO) is defined with an obliquity of 24.5° (22.5°), an eccentricity of 0.05 (0.05), and a longitude of perihelion of 90° (270°) [*DeConto and Pollard*, 2003]. Following the models of solar physics [*Gough*, 1981] and previous studies about Ordovician climate [*Pohl et al.*, 2014, 2015], the solar constant is decreased by 3.5% compared to its present value. The values for Ordovician pCO_2 remain a major uncertainty. They were necessarily higher than today, compensating for a weaker insolation, but climatic proxies [*Yapp and Poths*, 1992; *Rothman*, 2002; *Tobin and Bergström*, 2002; *Tobin et al.*, 2005; *Vandenbroucke et al.*, 2010a; *Pancost et al.*, 2013], climate models [*Herrmann et al.*, 2003, 2004], and long-term carbon cycle models [*Berner*, 1990; *François et al.*, 2005; *Berner*, 2006; *Young et al.*, 2009; *Nardin et al.*, 2011; *Goddéris et al.*, 2014] give scattered values ranging from less than 5 PAL to more than 20 PAL. In order to cover this wide spectrum, experiments are conducted for pCO_2 values between 3 PAL and 24 PAL.

2.3. Sensitivity Tests

2.3.1. One-Way Coupling Versus Asynchronous Coupling Method

Most experiments discussed in this study are conducted with the Earth system model described previously (i.e., the asynchronous coupling method; see section 2.1). Additional experiments are conducted with a simpler experimental design to allow comparison with previously published work and to test the sensitivity of our results to various parameters. Similar to previous studies [*Herrmann et al.*, 2003, 2004], we unidirectionally force the ice sheet model (GRISLI) with atmospheric outputs representative of ice-free conditions. As in the asynchronous coupling method, GRISLI updates its surface temperature and precipitation fields as a function of ice sheet height, through an adiabatic lapse rate for the temperature (5 K km^{-1}) and an exponential law for the precipitation (Clausius Clapeyron dependency), thus capturing the effect of the ice sheet on local climate. The one-way forcing method, however, differs from our asynchronously coupled model by lacking

ice sheet feedbacks on regional and global climates. The ice sheet model is not able to account, by itself, i.e., without being provided with additional climatic forcing fields, for larger-scale effects such as the impact of the ice sheet on the atmospheric circulation. It also significantly underestimates the regional cooling induced by the ice sheet by neglecting the strong ice-albedo positive feedback. For these one-way simulations, climatic forcing fields are computed using the method described previously (FOAM and then LMDZ). We use the cold summer orbital configuration (CSO), which is particularly favorable to Southern Hemisphere ice sheet growth. The resulting steady state ice sheets therefore represent the maximum land ice extent and volume that can be reached without considering land ice feedbacks on global climate.

2.3.2. Response of Ice Dynamics to Continental Topography

Published continental reconstructions do not necessarily concur with each other regarding the location of Ordovician highlands over Gondwana [e.g., *Blakey*, 2016; *Scotese*, 2016], and none of them provide numerical values for the altitude of these mountainous areas. In our baseline runs, we define mountainous areas based on *Blakey*'s [2016] Late Ordovician reconstruction (section 2.2.2), and we assign constant altitude of 2000 m to these highlands. To estimate the dependence of our modeling results on the large uncertainties in Ordovician topographic reconstructions, we run two additional sets of experiments involving a flat Gondwana supercontinent over the South Pole (constant altitude of 300 m) and a lowered topography where mountainous areas are set to 600 m altitude. For each of these tests, the one-way forcing method is used. LMDZ is run for each pCO_2 in a cold summer orbital configuration, using the appropriate topography, but keeping the sea surface temperatures previously simulated in our one-way baseline runs (section 2.3.1). GRISLI is subsequently forced using the LMDZ climatic fields. Using fixed sea surface temperatures allows to specifically investigate the impact of mountainous areas on the atmospheric circulation and thus on the patterns of the precipitation and temperature forcing fields provided to GRISLI, by avoiding ocean dynamics complex responses to changing topography.

2.3.3. Response of Ice Dynamics to Glacier/Bedrock Coupling

In spite of their limited spatial extent, ice streams today represent the most dynamic components of ice sheets, notably accounting for more than 90% of all the ice and sediment discharged by the Antarctic ice sheet [*Bennett*, 2003]. Ice streams consequently constitute a central component of the dynamic behavior of present ice sheets. In the model GRISLI, they are simulated using the shallow-shelf approximation (see section 2.2.1). In this context, the driving term for the ice flow computation is the basal sliding, which is computed as a function of basal shear stress and effective pressure, the latter as a function of the subglacial water pressure. Because shear stress and effective pressure are highly dependent on the geology of the subglacial environment, a sediment map is usually provided as a boundary condition to the model. However, the nature of the Ordovician continental surface is unknown over virtually the entire Gondwana supercontinent, challenging the accurate reconstruction of sediment thickness. The strength of the glacier/bed coupling therefore remains a major uncertainty in our deep-time modeling study, potentially biasing the modeled land ice volume and extent. In order to quantify the amplitude of this possible bias, we conduct a sensitivity test of the glacier/bed coupling strength by varying the basal dragging in the model. The basal dragging is the force generated by the friction between the flowing ice sheet and its bedrock, which hampers ice motion. In the model, the direction of basal dragging is opposite to that of basal velocity [*Ritz et al.*, 2001], and its value is a function of the latter [*Alvarez-Solas et al.*, 2011]:

$$\tau_b = -v^2 N U_b \tag{1}$$

where τ_b is the basal dragging, U_b is the basal velocity, N represents the effective pressure, and v^2 is an empirical parameter representing the basal friction coefficient in ice streams, the value of which will be varied. For these tests, the climatic forcing fields used in GRISLI are the same in all the experiments: we use the one-way forcing method, the cold summer orbit, and Blakey's topography [2016] with mountainous areas set to 2000 m.

3. Results

3.1. One-Way Experiments

To facilitate the comparison of our results with previous modeling studies [*Herrmann et al.*, 2003, 2004; *Lowry et al.*, 2014], we first conduct experiments that account neither for ice sheet feedback processes nor for orbital variations (see section 2.3.1). As expected, ice sheets of various extent and height are simulated, depending on the pCO_2 (Figure 2). The lower the pCO_2, the larger the ice sheet. The relationship between pCO_2 and land

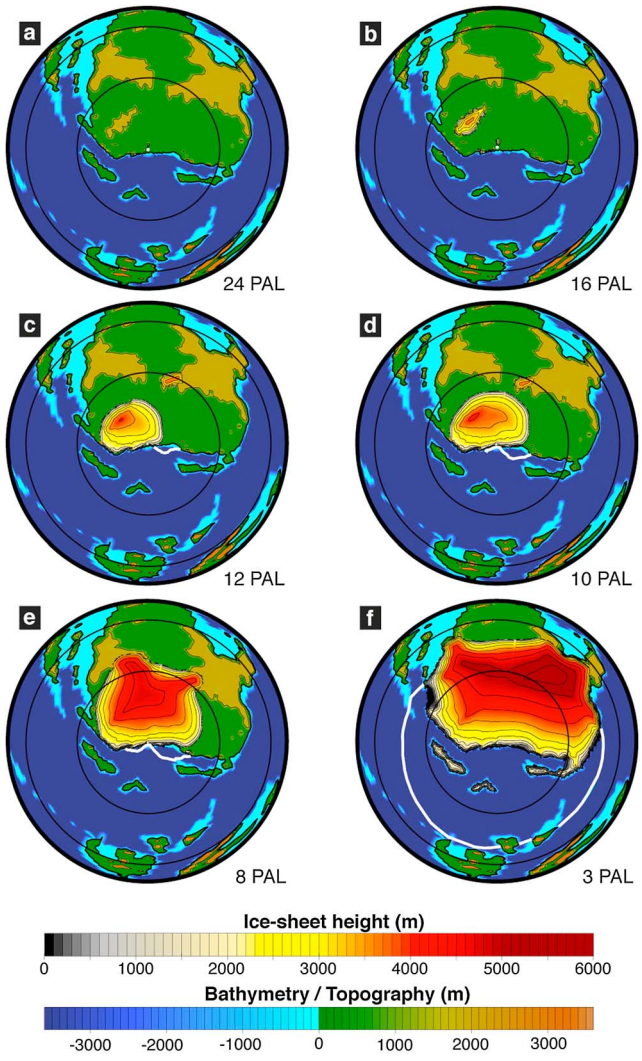

Figure 2. South polar projection maps of Late Ordovician steady state ice sheet heights (m) simulated at various CO_2 levels with the "one-way" forcing method, i.e., with no land ice feedbacks on global climate. For these simulations, the cold summer orbit is used. The thick white line corresponds to a mean annual sea ice fraction equal to 50%. Background shading is topography/bathymetry. Latitude is shown at 30° intervals.

ice volume is linear in a log-axis graph (Figure 3a, blue line). *Herrmann et al.* [2004] employed a similar experimental setup to run simulations on two Late Ordovician continental configurations from *Scotese and McKerrow* [1991]. They investigated the impact of several factors on glacial onset, i.e., pCO_2, sea level, and heat transport. Their set of experiments including a low sea level and a "normal" (versus "decreased") oceanic heat transport was typified by boundary conditions very close to the ones used in this study. As summarized in their Table 2, their simulation conducted at 15 PAL did not lead to glacial onset, whereas a continental-scale ice sheet was simulated at 8 PAL. Figure 2 reveals that in our models, (i) an ice sheet of limited spatial extent develops on polar highlands at 16 PAL, apparently indicating a glacial onset at higher CO_2 levels than *Herrmann et al.* [2004]. *Herrmann et al.* [2004], however, prescribed a flat continent, with altitudes set to 250 m on coastal grid points and 500 m everywhere else, compared to 2000 m for ancient orogens and 300 m elsewhere in our case. Interestingly, additional simulations with mountainous areas lowered to 600 m (see section 3.3.1) are typified by a glacial onset occurring at 8 PAL in our models, eventually providing a CO_2 threshold for glacial onset very comparable to the one proposed by *Herrmann et al.* [2004]; (ii) The ice sheet simulated at 8 PAL extends to ~60°S (Figure 2), which is in reasonable agreement with the extent simulated by *Herrmann et al.* [2004] for the same pCO_2 on their latest Ordovician reconstruction (see their Figure 6).

The experimental setup used by *Lowry et al.* [2014] was very comparable to the one of *Herrmann et al.* [2004]. Similar to *Herrmann et al.* [2004], climatic forcing fields were simulated using the GENESIS model on a flat topography under a cold Southern Hemisphere summer orbital configuration. In their simulations using a solar constant set to −2.5 % below present, *Lowry et al.* [2014] obtained a threshold CO_2 level for glacial inception below 3 PAL. Further accounting for early Paleozoic solar luminosity values raised the pCO_2 threshold to 4 PAL. Land ice growth did not occur at 8 PAL. This discrepancy between the results of *Herrmann et al.* [2004] and ours, on the one hand, and the ones of *Lowry et al.* [2014], on the other hand, may at least partly result from the choice of the vegetation cover. Here we use a barren soil, the albedo of which corresponds to a rocky desert (section 2.2.2). *Herrmann et al.* [2004] used no vegetation and intermediate soil color values. *Lowry et al.* [2014], on the contrary, coupled GENESIS to BIOME4, an equilibrium terrestrial vegetation model simulating the changing distribution of 28 modern biome types in response to climatic forcing. Sensitivity tests demonstrated that ice sheet initiation was sensitive to vegetation (supporting information of *Lowry et al.* [2014]).

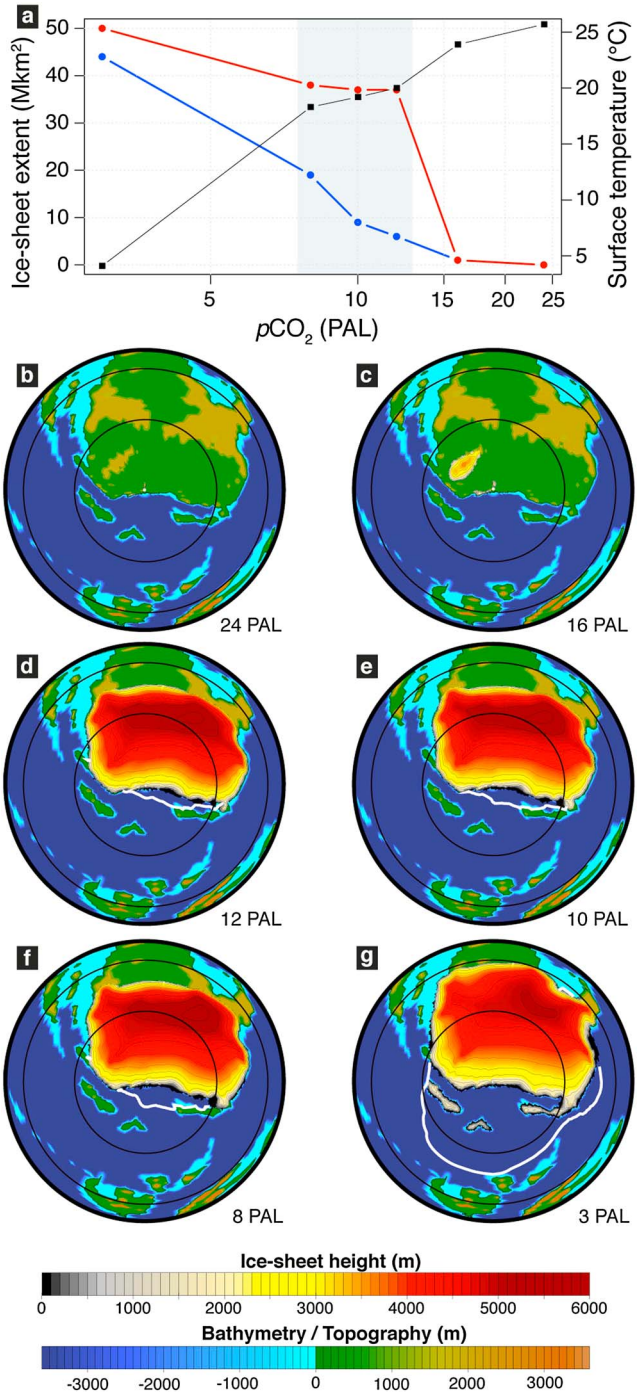

Figure 3. Ice sheet results at various CO_2 levels. (a) Ice sheet extent simulated under a cold summer orbit without taking ice sheet feedbacks on climate into account (one way, blue line) and with our asynchronous coupling procedure accounting for orbital variations and ice sheet feedbacks (red line). Global mean annual surface air temperature (black line, right *y* axis) is displayed for the asynchronous coupling method only, once the ice sheet obtained steady state with global climate. (b–g) South Pole projection maps of Late Ordovician equilibrium ice sheet heights (m) simulated at each CO_2 level, using the asynchronous coupling method accounting for orbital variations and ice sheet feedbacks. Background shading is topography/bathymetry. The thick white line corresponds to a mean annual sea ice fraction equal to 50%. Latitude is given at 30° intervals. See Figure 8 for a time series of land ice growth. The grey rectangle in Figure 3a indicates the domain where ice sheets sustain in an otherwise relatively warm climate; see section 4.2.

The use of a bare ground induced larger ice volumes and surface area. In some time slices of the Phanerozoic, a barren soil raised the CO_2 threshold for glaciation.

It is more difficult to directly compare our results with the work from *Herrmann et al.* [2003], who conducted their experiments for a narrower pCO_2 range (8–12 PAL) and focused on the sensitivity of the modeled ice sheet volume to the obliquity forcing. Orbital variations are not considered in our one-way experiments, though they are in our asynchronously coupled runs (see section 2.1).

It appears that using the one-way forcing method, our models compare relatively well with the results of *Herrmann et al.* [2004]. In the simulations of *Lowry et al.* [2014], glacial onset occurs for slightly lower CO_2 levels, possibly due to their modern vegetation cover.

3.2. Accounting for Ice Sheet Feedback Processes

Simulations are run with the same models and boundary conditions, using the asynchronous coupling method accounting for orbital variations and, for the first time, for the feedbacks of the ice sheet on global climate. Changes in ice surface elevation and extent affect surface air temperatures and atmospheric circulation and vice versa (see section 2.1). Figure 3a displays the equilibrium surface air temperature (black line) and ice sheet extent (red line) simulated at various pCO_2 levels. At 24 PAL, the climate is warm (global, mean annual surface air temperature of ~25.7°C, Figure 3a) and no land ice is observed over the South Pole (Figure 3b). When CO_2 is decreased to 16 PAL, the climate cools slightly (by 1.8°C) and small ice caps appear on the polar highlands (Figure 3c). When CO_2 is lowered to 12 PAL, an ice sheet suddenly expands to the midlatitudes (~45°S, Figure 3d) and global temperature decreases by 3.9°C (from 23.9 at 16 PAL to 20.0°C at 12 PAL, Figure 3a). After this first step of sudden ice sheet growth, the position of the ice front stabilizes and ice sheets of similar size and volume are simulated at 12, 10, and 8 PAL (Figures 3a, 3d–3f). When CO_2 is further lowered to 3 PAL, global temperature suddenly plummets by ~14°C (Figure 3a) inducing a second-step latitudinal expansion of the land ice by a further 15° (Figures 3a and 3g), whereby the continental ice sheet reaches the tropical realm (30°S). Sea ice—previously confined to higher paleolatitudes—expands to 45°S (Figure 3g).

During the first step, global climate suddenly shifts from a greenhouse (pCO_2 > 12 PAL) to an icehouse mode with the land ice front resting at the midlatitudes (12–8 PAL, Figures 3d–3f). Despite the continental configuration favoring a strong continentality over the southern high latitudes, analysis of the mechanisms of incipient glaciation reveals that accumulation is never the limiting factor for land ice growth (Figure 4). The latter is, on the contrary, driven by lack of ablation (Figure 4), as reported for the Laurentide ice sheet during the Last Glacial Maximum [*Bonelli et al.*, 2009]. The Ordovician ice sheet nucleates near the South Pole on highlands where freezing persists during the austral summer season, i.e., where ablation is virtually zero throughout the year. Once the ice cover is sufficiently large, the ice-albedo and height mass balance feedbacks amplify the extension of the zero-ablation zone (Figure 4). The ice sheet expands equatorward until it reaches the midlatitudes, where it stabilizes from 12 to 8 PAL (Figures 3d–3f). This apparent contradiction between pCO_2 decrease and unchanged land ice extent, between 12 PAL and 8 PAL (grey domain in Figure 3a), is caused by higher ablation rates in the warmer midlatitudes (supporting information), limiting the ice line close to 45°S. The nonlinear extension of the land ice simulated in this first step is comparable, to some extent, to the Pleistocene glacial cycles, during which interstadials (when only Greenland was covered by ice) were succeeded by stadials when the Laurentide ice sheet suddenly extended to 40°N [*Ehlers and Gibbard*, 2007]. The ice sheet extension of the second step, simulated at 3 PAL, relies on a specific mechanism. *Pohl et al.* [2014, 2015] showed that there is a threshold CO_2 value, below which Ordovician climate abruptly shifts from a warm climatic equilibrium with no sea ice in the Northern Hemisphere to a much colder state with sea ice extending down to the midlatitudes. They attributed this climatic instability to the particular ocean dynamics developing in the mainly oceanic Ordovician Northern Hemisphere. At 3 PAL, the sudden spread of sea ice to the midlatitudes (Figure 3g), associated with the crossing of this climatic tipping point, induces a global climate cooling by 14°C (Figure 3a). This abrupt cooling leads in turn to the advance of the continental ice front to the tropical latitudes (Figure 3g).

The quasi-absence of ice shelves in our model runs (Figure 3) results from the very strong ablation outside the grounded ice sheet on the one hand (Figure 4h) and from the poorly constrained Ordovician bathymetry on the other hand. The South Pole, in particular, is the single area typified by lower ablation rates (Figure 4h). There, however, open ocean conditions suddenly succeed to the Gondwana peneplain continent in our

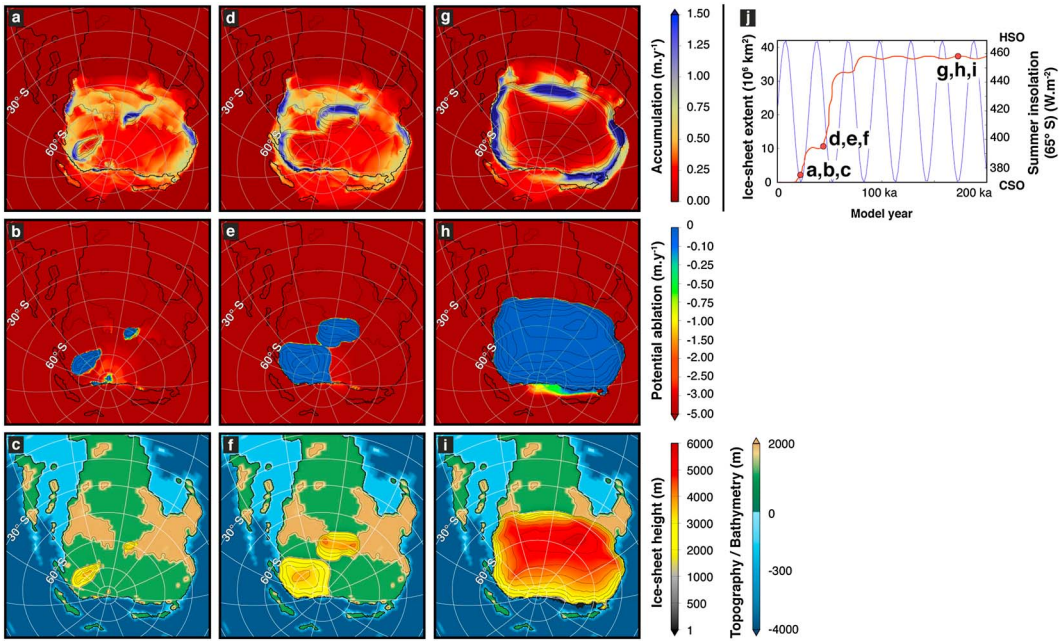

Figure 4. Respective contributions of accumulation and ablation to the growth of the Ordovician ice sheet, illustrated by three snapshots taken from the simulation conducted with ice sheet feedbacks and orbital variations at 12 PAL, at (a–c) 22 ka, (d–f) 44 ka, and (g–i) 173 ka. Latitude is shown at 15° intervals, and land ice cover is systematically displayed through ice sheet height isolines. (j) The three snapshots (22, 44, and 173 ka) are placed on the time series of ice sheet growth (similar to iter 9 in Figure 1), where the red curve represents the increasing extent of the ice sheet through the ice sheet model integration time (200 ka) and the blue curve the oscillations of the orbital forcing between the CSO and HSO end-members (see section 2.2.2). Comparing the three plots provided for each selected model year reveals that accumulation is never the limiting factor for ice growth, because the positive accumulation zone always exceeds the ice sheet extent (Figures 4a, 4d, and 4g). On the contrary, potential ablation is very strong outside of the ice sheet edges, thus limiting further ice sheet extension. The enlargement of the zero-ablation zone (Figures 4b, 4e, and 4h)—driven by local cooling due to the ice-albedo and height mass balance positive feedbacks—allows the ice sheet to develop through the elapsing simulation (Figures 4c, 4f, and 4i).

bathymetric reconstruction, with no fine-scale slope in between (see Figure 4c), which implies strong oceanic melt rates under the shelves in the model (see section 2.2.1). Moreover, there are very few embayments to favor the development of ice shelves. Given that floating ice does not contribute to sea level variations when it forms or breaks up, uncertainties regarding the extent of simulated ice shelves do not alter our estimates of the glacioeustatic fall discussed in section 4.4.

3.3. Sensitivity Analysis

We here quantify the impact of the basal dragging and of the bedrock topography on the geometry of the simulated ice sheet. Because running our asynchronously coupled model for each of these additional experiments would be time consuming and expensive, we here use the one-way forcing method and we conduct simple, first-order sensitivity tests under the cold summer orbital configuration. We previously demonstrated that using the one-way method, a very low CO_2 level (3 PAL) is required to simulate a continental-scale ice sheet similar to the ice sheet modeled with our more sophisticated setup (compare Figure 2f with Figures 3d–3f). We therefore conduct most of our sensitivity tests at 3 PAL, in order to ensure that the results of these tests are instructive regarding the geometry of such a continental-scale ice sheet.

3.3.1. Sensitivity to Topography

The most straightforward effect of a mountainous area is to allow the continental surface to intercept the 0°C isotherm, where a flat topography would not, thus making the nucleation of ice centers easier. Conversely, considering lowered relief is expected to shift the threshold for glacial onset toward lower pCO_2 values. With the default topography used in our baseline runs, glacial onset takes place at 12 PAL (Figure 2). When mountains are lowered to 600 m, the threshold pCO_2 value for glaciation is effectively shifted to 8 PAL. With a flat topography, land ice nucleates only at 3 PAL over Gondwana.

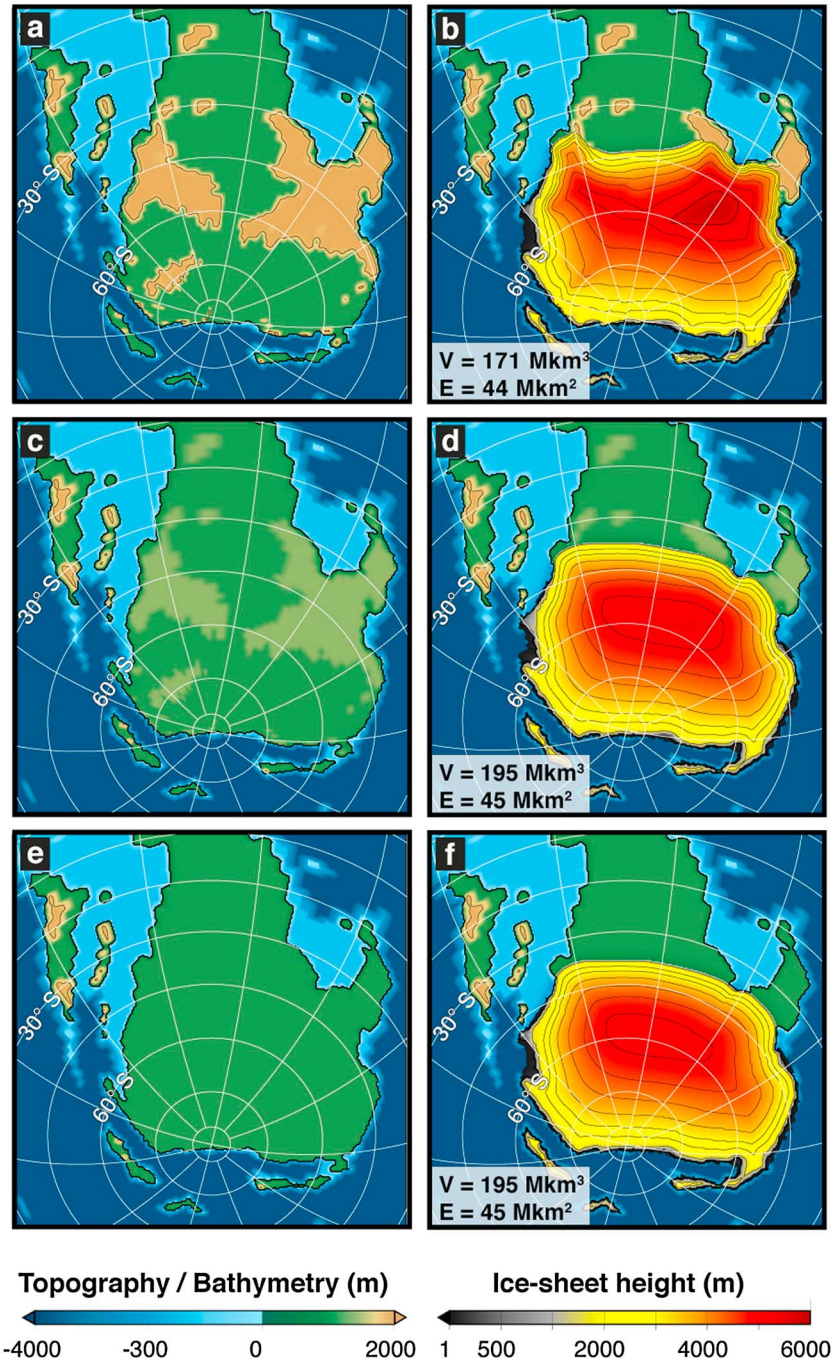

Figure 5. Sensitivity of simulated ice sheet height and extent to topography. Each row corresponds to an experiment. (a, c, and e) The topography used in the model. (b, d, and f) The ice sheet height simulated at equilibrium together with simulated ice sheet volume (V, 1 $Mkm^3 = 10^6\ km^3$) and extent (E, 1 $Mkm^2 = 10^6\ km^2$). For these simulations, we use the one-way forcing method and the cold summer orbital configuration.

Figure 5 compares equilibrium ice sheets simulated at 3 PAL, using each topography. Although topography significantly impacts the ice sheet geometry, equilibrium ice sheet extent is almost insensitive to topography. Lowered mountains (Figures 5c and 5d), or even a flat Gondwana supercontinent (Figures 5e and 5f), alter the modeled land ice area by no more than 4.5%. The maximum latitudinal extent of the ice sheet, in particular, is remarkably stable. The regional advance of the ice front toward lower latitudes in the center of Gondwana, when topography is flattened (compare Figure 5b with Figures 5d and 5f), results from the changing atmospheric circulation when highlands are removed. Zonal winds are not hampered by relief any more, and they

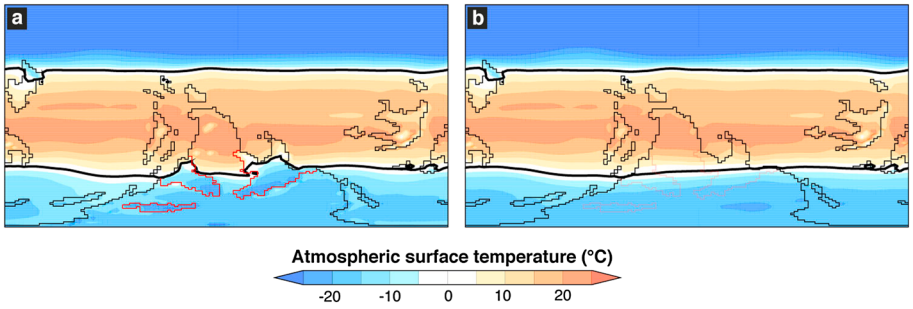

Figure 6. Austral summer (December, January, and February average) surface air temperature simulated using the one-way forcing method under CSO, land ice-free conditions using (a) the default topography reconstructed from Blakey (2000 m) and (b) the flat topography. Continental mass outlines are shown with the black, stepped, thin black lines. In Figure 6a, main mountains typifying the topography used over Gondwana during the simulation are shown with red, stepped lines. In Figure 6b, the topography is set to 300 m everywhere over Gondwana during the simulation but the location of former relief is mapped in order to facilitate the comparison with Figure 6a. In both cases, the thick black line stands for the 0°C isotherm.

allow the austral summer 0°C isotherm to advance toward the tropics (Figure 6). There is, however, quasi-cancelation between this regional extension of the ice sheet and the retreat of the ice sheet from surrounding mountainous areas due to the warming effect of the lapse rate for lowering topography (Figures 5b, 5d, and 5f). As a result, the extent of the ice sheet only slightly increases (+1 Mkm^2, Figures 5b, 5d, and 5f) and the land ice volume follows (+24 Mkm^3, Figures 5b, 5d, and 5f).

3.3.2. Sensitivity to Basal Dragging

Land ice thickness simulated in our baseline runs reaches 6000 m over extensive areas, and the ice sheet systematically displays very steep flanks (Figure 7a). These characteristics are comparable with the results from *Herrmann et al.* [2004] (see their Figure 6), but they are not realistic when compared to present-day Antarctic [e.g., *Fretwell et al.*, 2013] or LGM Laurentide [e.g., *Heinemann et al.*, 2014] ice sheets. Furthermore, the model simulates virtually no ice stream zones over the entire Gondwana supercontinent (Figure 7b), which is at odds with the sedimentary record of the Ordovician glaciation [e.g., *Denis et al.*, 2007; *Ghienne et al.*, 2007]. These discrepancies arise from weakly dynamic ice sheet, notably resulting from the absence of topographic undulations in our poorly constrained Ordovician topographic reconstruction. The latter includes topographic classes with constant elevation, with no valleys to promote fast-flowing ice streams (see section 2.2.1). In order to quantify this bias, we conduct additional experiments using the basal dragging parameterization developed by *Alvarez-Solas et al.* [2011] to account for the ice sheet instability. This basal dragging code was successfully applied to study the Heinrich event 1 [*Alvarez-Solas et al.*, 2011]. It uses, in the ice stream zones, a basal dragging coefficient v^2 (see section 2.3.3) that is lower than the one used in our baseline runs. It is also less restrictive regarding the conditions required to generate ice stream zones. In contrast to the basal dragging parameterization used in our baseline runs, it uses a sediment map and allows ice streams to develop over areas with very limited basal water content if the bedrock is covered by sediments. For the Ordovician, no detailed lithologic maps of Gondwana are available, but some areas were undoubtedly covered by sediments [*Denis et al.*, 2007]. In the absence of better constraints, we here impose a uniform sediment cover over the supercontinent, and we set the basal friction coefficient for ice streams to $v^2 = 2 \times 10^{-5}$ (dimensionless), following *Alvarez-Solas et al.* [2011]. Results obtained with this setup are displayed in Figures 7c and 7d.

Ice sheet geometry simulated at 3 PAL with the *Alvarez-Solas et al.*'s [2011] parameterization shows large differences with our baseline simulation (Figures 7a and 7c). The equilibrium ice sheet extent does not change, but the ice sheet flattens and simulated ice volume decreases from 171 Mkm^2 to 99 Mkm^2, eventually representing only 58% of the volume simulated in the baseline experiment (Figures 7a and 7c). The constant ice sheet extent, on the one hand, is due to the unchanged climatic forcing. Decreased ice volume, on the other hand, results from high land ice velocities over extensive ice stream zones (Figures 7b and 7d). Figure 7e (black points) shows the results from additional experiments with various values of the basal dragging coefficient v^2. It confirms that the strength of the glacier/bedrock coupling impacts the simulated ice volume but not the ice sheet extent. These results are in agreement with the studies of *Clark and Pollard* [1998] and *Tabor and Poulsen* [2016], who simulated similar Laurentide ice sheet extents, but different volumes, as sediment cover changed across the middle Pleistocene transition (~ 0.9 Ma). We also conduct an experiment featuring a

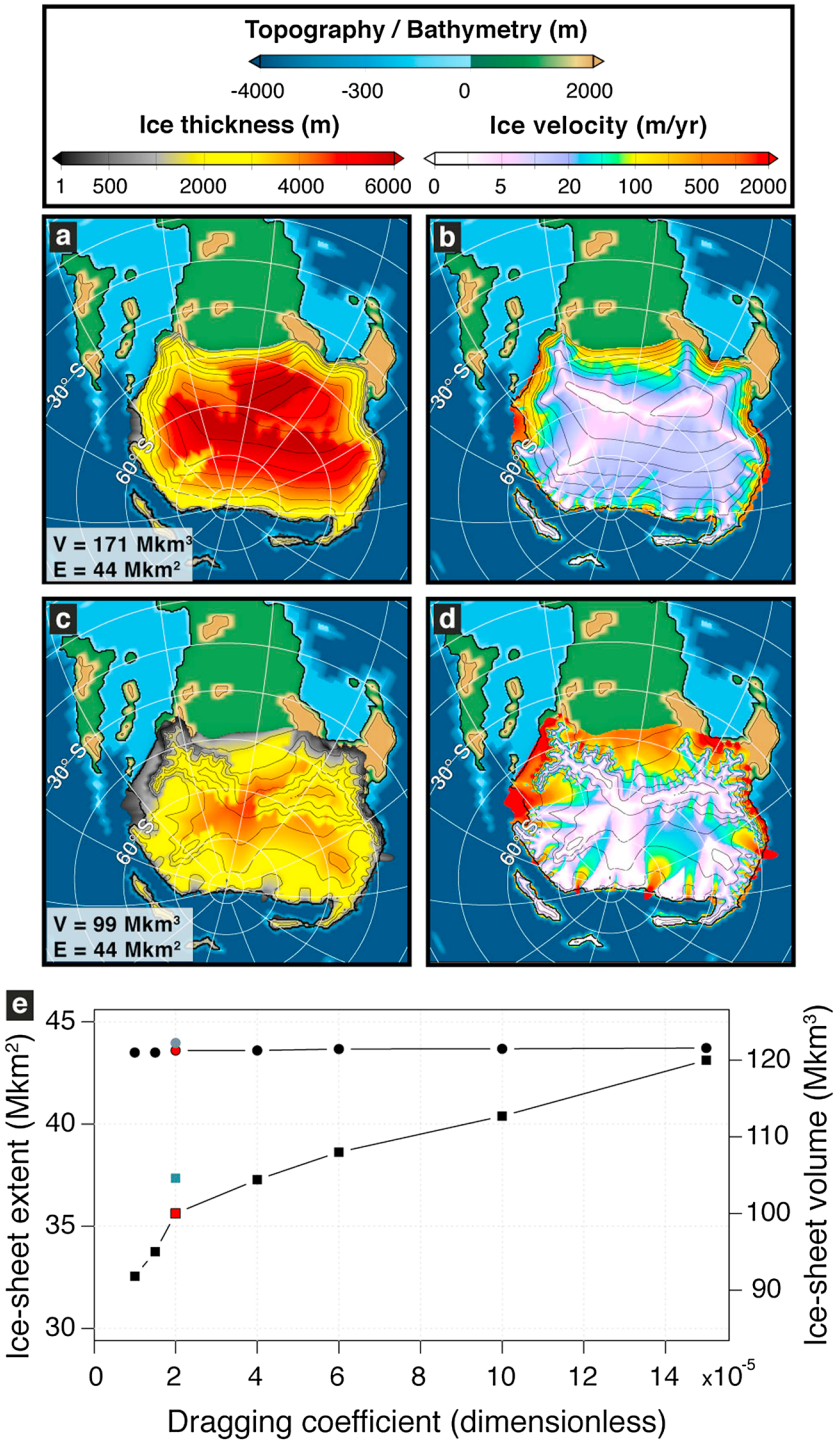

Figure 7. Sensitivity of simulated land ice thickness and extent to basal dragging coefficient. These simulations are conducted using the one-way forcing method and a cold summer orbit. (a, b) Results from our baseline experiments. (c, d) Results obtained using the basal dragging parameterization developed by *Alvarez-Solas et al.* [2011] with the standard basal dragging coefficient: $v^2 = 2 \times 10^{-5}$. Isolines correspond to ice sheet height. They are displayed every 500 m. (e) The dependence of simulated ice sheet extent (circles) and volume (squares, right *y* axis) on the basal dragging coefficient, using the parameterization from *Alvarez-Solas et al.* [2011]. Red circles and squares show the values obtained with the standard basal dragging coefficient of 2×10^{-5}, which results are displayed in Figures 7c and 7d. Grey circles and squares stand for the simulation using the same coefficient and a sediment map in addition. Black symbols stand for simulations where the value of the basal dragging coefficient is varied (*x* axis), with no sediment map.

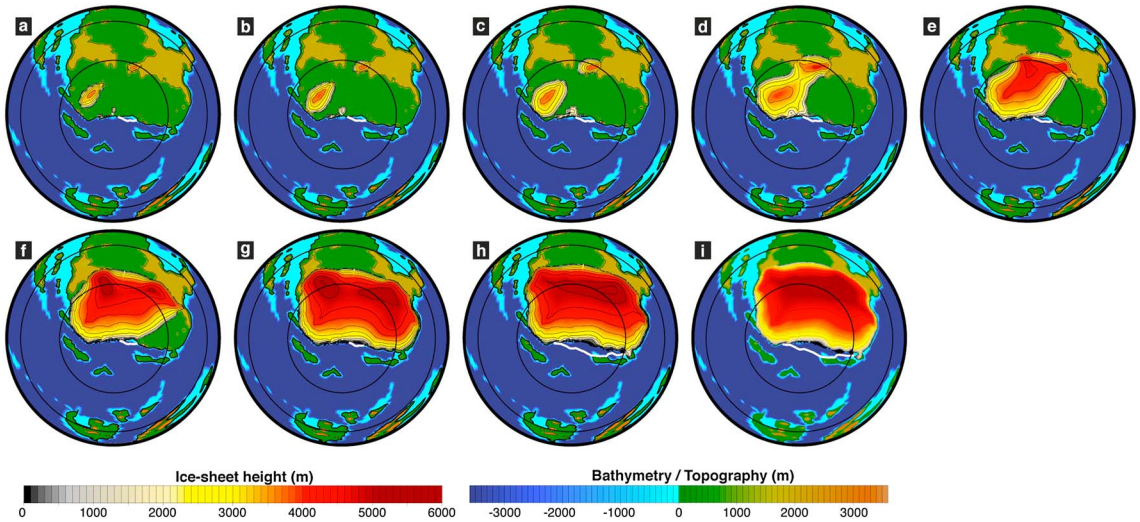

Figure 8. Ice sheet height simulated at 12 PAL, under varying orbital forcing, throughout the successive asynchronous coupling steps (south polar projection maps). (a–i) The largest ice sheet simulated during each one of the successive iterations, which is subsequently returned as a boundary condition in the climate models to simulate the next ice sheet extent (see section 2.1). Background shading is topography/bathymetry. Latitude is shown at 30° intervals.

partial sediment cover. This is a first-order test with sediments present everywhere in topographic lows (i.e., a peneplain continent) but absent where the elevation of the terrain is above 300 m. Highlands are considered as rocky bedrock, and they are characterized by the very strong glacier/bedrock coupling typifying inland ice in GRISLI. This spatialization of the basal dragging strength induces differential sliding over Gondwana. Results (Figure 7e, grey points) show that including a sediment map does not critically impact our results.

In summary, sensitivity tests show that uncertainties in topographic reconstructions impact the threshold CO_2 value for glacial onset. Accounting for ice streams—fast-moving ice regions, demonstrated to have been present from the Upper Ordovician record [*Moreau et al.*, 2005; *Denis et al.*, 2007; *Le Heron et al.*, 2007; *Ghienne et al.*, 2007; *Denis et al.*, 2010; *Ravier et al.*, 2015]—further demonstrates that the land ice volume simulated in our baseline runs has to be considered with caution. The two opposite and relatively extreme parameterizations tested here, leading to a weakly dynamic (in our baseline simulations) and especially dynamic (using the basal dragging dependence on sediments from *Alvarez-Solas et al.* [2011]) ice sheet, provide, respectively, maximum and minimum estimates for the volume of the Ordovician ice sheet. Irrespective of the topography and basal dragging parameterization, the modeled ice sheet extent, by contrast, turns out to be remarkably stable and thus reliable.

4. Discussion

4.1. Constraining Ice Sheet Extent

When accounting for the ice sheet feedbacks on Ordovician climate, the ice sheet expands to the low latitudes rather than being restricted in the polar area ($\geq$ 60°S). This is an important result compared to the earlier models that omitted ocean-atmosphere-ice sheet interplays, such as those of *Herrmann et al.* [2003, 2004]. In our advanced models, a single ice sheet of large extent covers Gondwana from the South Pole to the middle-to-tropical paleolatitudes (Figure 3). The time series of ice sheet growth at 12 PAL, shown in Figure 8, reveals that highlands facilitate independent glacial centers to simultaneously nucleate over the Pole and at 60°S during the primary stages of glacial growth (Figures 8a–8c). However, such glacial centers are not initiated at middle-to-tropical paleolatitudes, where South Africa and South America were situated 445 Ma ago [*Torsvik and Cocks*, 2013], in any of our simulations. Furthermore, results from our Earth system model accounting for ice sheet feedback processes reveal that the local cooling associated with the growth of these glacial centers rapidly induces their coalescence into a single, continental-scale ice sheet (Figures 8c, 8d, and Figure 3). In our simulations, the persistence of independent ice sheets over Gondwana is not a sustainable land ice state. This result contradicts the hypothesized configuration that features multiple, individual ice sheets in North Africa, South Africa, and South America [e.g., *Le Heron and Dowdeswell*, 2009]. The sensitivity analysis we conducted (section 3.3) further reveals that the simulated ice sheet extent is a robust

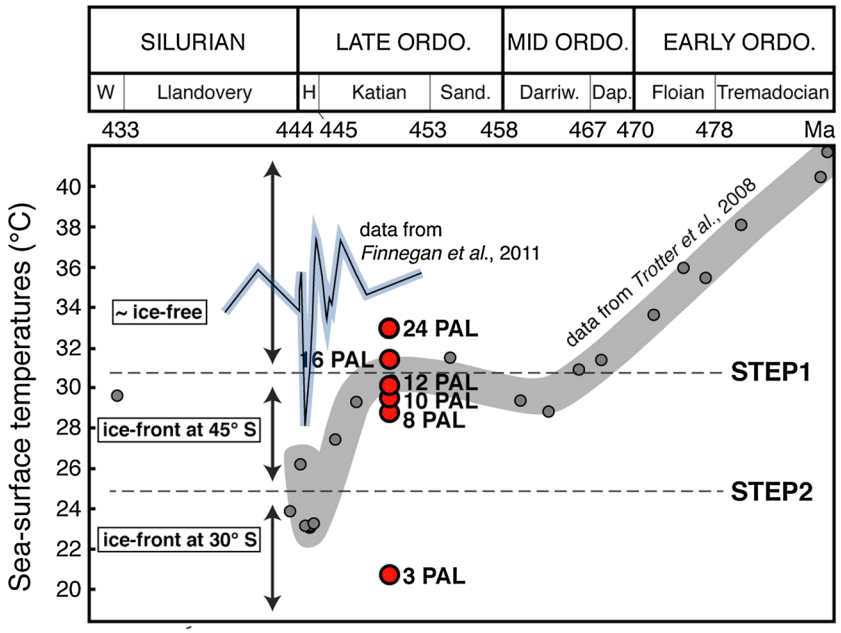

Figure 9. Comparison of tropical sea surface temperatures (SSTs) reconstructed based on $\delta^{18}O$ [*Trotter et al.*, 2008] and $\Delta^{47}CO_2$ [*Finnegan et al.*, 2011] data with annual mean tropical (30°S–30°N) SSTs simulated for the Late Ordovician once ice sheets in steady state (red circles), using our asynchronous coupling method accounting for ice sheet feedback processes and for orbital variations. Modified after *Trotter et al.* [2008] and *Finnegan et al.* [2011]. *Dap.*: *Dapingian*; *Darriw.*: *Darriwilian*; *Sand.*: *Sandbian*; *H*: *Hirnantian*; *W*: *Wenlock*.

feature that is critically dependent neither on the topographic reconstruction nor on a specific basal dragging parameterization. Our results are also supported by the study of *Lowry et al.* [2014], who simulate a single ice sheet over Gondwana with a different asynchronous coupling method and other climate and ice sheet models.

4.2. Glacial Onset in a Warm Climate

The buildup of the ice sheet, in response to a decrease in atmospheric forcing, is not linear. Between 16 PAL and 12 PAL, the ice sheet suddenly extends from the South Pole to the midlatitudes (Figure 3a), whereas tropical sea surface temperatures decrease by no more than 1.3°C (Figure 9). This nonlinear response suggests that the development of a large-scale ice sheet during the Ordovician could have occurred in conjunction with a moderate tropical sea surface temperatures signal, the amplitude of which would be within the error bars of routine geochemical analyses [e.g., *Finnegan et al.*, 2011] and thus potentially below the detection limits. This further implies that warm tropical Ordovician seas [*Trotter et al.*, 2008; *Finnegan et al.*, 2011] and geological evidence for glacioeustatic events [*Loi et al.*, 2010; *Turner et al.*, 2012; *Dabard et al.*, 2015; *Rasmussen et al.*, 2016] are not mutually exclusive (30.3°C at 12 PAL, Figure 9). Interestingly, experiments using a lowered topography (section 3.3.1) are typified by a glacial onset occurring at 8 PAL (instead of 12 PAL). They show that the unexpected glacial inception in a warm climate does not result from the high relief characterization of our baseline runs.

4.3. Toward an "Early Paleozoic Ice Age"

Trotter et al. [2008] demonstrated that tropical SSTs steadily cooled through the Early Ordovician, reaching present-day levels that were subsequently sustained during the Middle and Late Ordovician, followed by a sudden cooling by ~7°C during the latest Ordovician (Figure 9). Several arguments support the validity of these data. *Nardin et al.* [2011] in particular, using a coupled climate-carbon model, showed that changes in Ordovician paleogeography, along with variations in the surface area of outcropping fresh volcanic rocks, induce a long-term decrease in atmospheric CO_2. This provides a potential mechanism for the cooling pattern demonstrated by *Trotter et al.* [2008]. *Trotter et al.*'s [2008] data are also in good agreement with other published geochemical data for the Late Ordovician and for the Silurian, respectively, from *Buggisch et al.* [2010] and *Wenzel et al.* [2000]. Moreover, recent clumped-isotope data from tropical latitudes

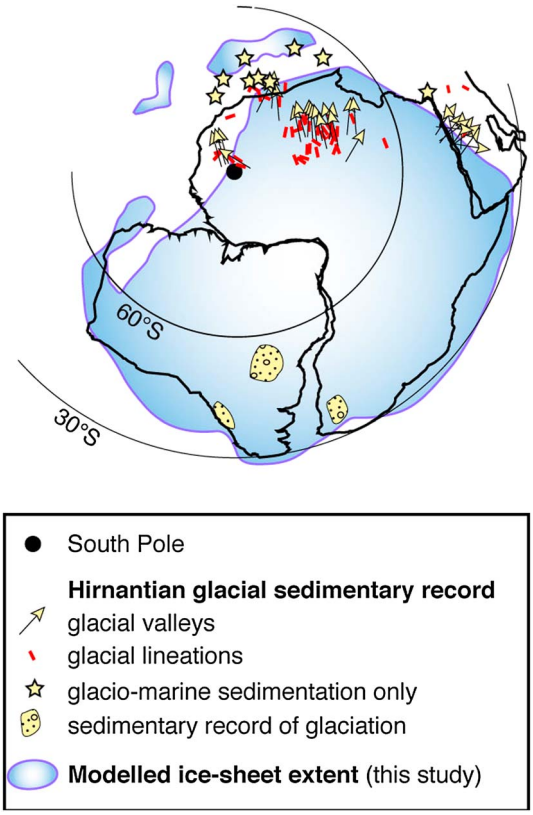

Figure 10. Comparison of the Hirnantian glacial sedimentary record with the ice sheet extent simulated at 3 PAL using our coupling method accounting for ice sheet feedbacks on global climate and for orbital variations. Data from North Africa are from *Ghienne et al.* [2007], and data from South America and South Africa are from *Díaz-Martínez and Grahn* [2007]. Continent outlines are taken from *Torsvik and Cocks* [2009].

[*Finnegan et al.*, 2011], although they are differently calibrated against the absolute temperature scale, display a similar temperature drop of 5 to 7°C during the latest Ordovician Hirnantian (Figure 9).

Figure 9 shows that the absolute values of tropical SSTs reconstructed by *Finnegan et al.* [2011] are systematically higher than those modeled in this study; this applies for our entire pCO_2 range, except for the Hirnantian where modeled and proxy-based SSTs align and correspond to a pCO_2 drop to 8 PAL in the model. Nonetheless, the generally unaligned SSTs (Figure 9) constitute a major discrepancy between *Finnegan et al.*'s [2011] data and our model runs. *Finnegan et al.* [2011] suggest the presence of large land ice volumes well before the Hirnantian, during the Katian, whereas the comparison between their SSTs and our simulations implies CO_2 levels that would have remained above 24 PAL and thus associated with ice-free conditions until the latest Ordovician, i.e., the Hirnantian. The modeled "Step 2" glaciation never occurred, based on these data. Simulated tropical SSTs are, however, in much better agreement with the range of absolute values presented by *Trotter et al.* [2008]. Comparison with Trotter's data suggests that ice sheet growth may have occurred as early as the Middle Ordovician (Figure 9). Taken at face value, our results, combined with these data, indicate a Darriwilian age for the glacial onset (between 16 and 12 PAL, *step 1* in Figure 9). The second step in ice sheet expansion would then correspond to the Hirnantian glacial maximum (3 PAL, *step 2* in Figure 9). Our modeled results are also in agreement with the amplitude of drop in SSTs during the Hirnantian that is suggested in both of these proxy data studies [*Trotter et al.*, 2008; *Finnegan et al.*, 2011], when we decrease CO_2 from 8 PAL to 3 PAL.

Such a straight model-data comparison has to be interpreted cautiously. In addition to potential bias in the data (e.g., dating or preservation issues), simulated absolute values are highly model dependent and may also be biased due to large uncertainties in Ordovician boundary conditions (see section 3.3). Comparing our modeling results with the long-term Ordovician climatic trend proposed by *Trotter et al.* [2008] is nevertheless instructive, as it suggests a Darriwilian glacial onset, which agrees with recently published studies that report glacioeustatic signals in the Darriwilian rock record [*Turner et al.*, 2012; *Dabard et al.*, 2015; *Rasmussen et al.*, 2016] and with paleontological studies that suggest pre-Sandbian cooling [*Vandenbroucke et al.*, 2009], and it provides physical mechanisms for the latest Ordovician glacial maximum and associated sudden climate cooling [*Trotter et al.*, 2008; *Finnegan et al.*, 2011]. Besides this interesting match with geochemically inferred tropical SSTs, our Katian estimates (8–12 PAL, Figure 9) match relatively well the ~8 PAL pCO_2 proposed by *Pancost et al.* [2013] based on the analysis of isotope fractionation between organic and inorganic carbon during photosynthesis (ϵ_p). Furthermore, the modeled spatial ice sheet extent at 3 PAL is overall consistent with the Hirnantian glacial sedimentary record (Figure 10). Discrepancies with shallow-shelf deposits from Turkey can be explained, as glacioeustatic emersion in such environments is not accounted for in our modeling procedure. In addition, using micropaleontological assemblage data to reconstruct climatic belts, *Vandenbroucke et al.* [2010a, 2010b] demonstrated that the Polar Front shifted in latitude from the Sandbian (460 Ma) to the Hirnantian (~440 Ma), reaching 40°S during the latest Ordovician. Comparing these Hirnantian data with the modeled climatic belts (Figure 11) reveals that again, the models best fit the data at 3 PAL. Taken

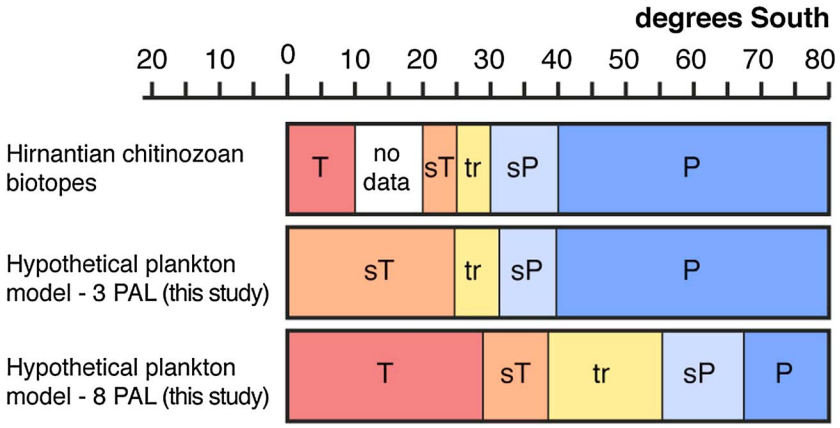

Figure 11. Comparison of Ordovician proxy-derived climatic estimates with values simulated with our asynchronous coupling method once the ice sheet reached steady state with global climate. Southern Hemisphere climatic belts reconstructed based on Hirnantian chitinozoan marine zooplankton data [*Vandenbroucke et al.*, 2010a, 2010b] are compared with climatic belts inferred from modeled SSTs. Abbreviations are plankton province names: *P*: *polar*; *sP*: *subpolar*; *tr*: *transitional*; *sT*: *subtropical*, and *T*: *tropical*. In our model predictions, the boundary between two plankton provinces is defined as the latitude at which the mean annual, latitudinally averaged SSTs simulated in the Southern Hemisphere reach the temperature threshold separating the two provinces in the present-day ocean. The reader is referred to *Vandenbroucke et al.* [2010a] for more details about the methods (see their Figure 1).

as a whole, our results suggest a protracted glaciation beginning as early as the Middle Ordovician Darriwilian and featuring a glacial maximum during the Hirnantian. By supporting the existence an ice sheet over the supercontinent Gondwana during most of the Middle and Late Ordovician, our results support the emerging paradigm of a protracted "Early Paleozoic Ice Age" [*Page et al.*, 2007].

4.4. Ice Volume Analysis

We calculate the glacioeustatic sea level fall associated with growing ice sheets using the methods employed by *Horton et al.* [2007] and *Horton and Poulsen* [2009]. First, the equivalent volume of water is estimated by multiplying modeled volume of ice above the flotation level by the ice density value (0.917). Then, we convert the water equivalent to an isostatically adjusted sea level equivalent (IASLE), by dividing the water equivalent by the Late Ordovician ocean surface area (~413 Mkm^2 at 450 Ma) and subsequently correcting the result for the response of the oceanic lithosphere to seawater loading/unloading. To that end, we multiply the result by $(1 - k)$, where k is the ratio of seawater density to oceanic lithosphere density ($k = 0.284$). Using results from our baseline runs, this simple calculation provides estimates of ~220 m between 12 and 8 PAL (step 1, Middle Ordovician) and ~250 m at 3 PAL (step 2, latest Ordovician Hirnantian). The sensitivity tests conducted in section 3.3.2 reveal that these values constitute uppermost estimates. The calculated minimum estimates are, respectively, 125 and 145 m.

Loi et al. [2010], using a backstripping procedure on the margin of Gondwana (Bou Ingarf section, Anti-Atlas, Southern Morocco), estimated an upper Hirnantian sea level fall of ~70 m. However, they explain that this sea level fall does not correctly represent the total ice volume stored over Gondwana during the latest Ordovician Hirnantian. It does not account for land ice stored over Gondwana before the Hirnantian climax. *Loi et al.* [2010] therefore estimate that the amplitude of the sea level fall would have reached nearly 150 m relative to the preglaciation (late Katian) datum [see also *Haq and Schutter*, 2008], and they note that this is a lower end estimate due to the incompleteness of the glacial sedimentary record. Moreover, recent studies [*Raymo et al.*, 2011; *Stocchi et al.*, 2013] demonstrated that the relationship between ice sheet growth and relative sea level fall is less linear than thought previously. Results obtained by *Stocchi et al.* [2013] on the onset of the Antarctic glaciation at the Eocene-Oligocene transition notably suggest that the near-field sea level change accompanying the growth of a continental-scale ice sheet is expected to strongly deviate from the global eustatic signal. Due to crustal deformation and gravitational perturbations, relative sea level around Antarctica *rose* in response to the buildup of the ice sheet. In the same way, the sea level fall documented by *Loi et al.* [2010] along the margin of Gondwana (150 m) may significantly underestimate Late Ordovician eustatic variations and should be considered as a lower end-member. Furthermore, recent clumped-isotope data from *Finnegan et al.* [2011] suggest that the Hirnantian ice volume may have reached twice that of the LGM, potentially

representing a water volume stored on land equivalent to 240 m sea level fall. It appears that our simulation run at 3 PAL eventually provides a total ice volume equivalent to 145 to 250 m sea level fall relative to ice-free conditions during the Hirnantian, thus in the same order of magnitude as most recent estimates inferred from sedimentological and geochemical data.

Ice volumes modeled between 12 and 8 PAL (125 to 220 m), on the contrary, are clearly much higher than the Middle Ordovician estimates reported by *Dabard et al.* [2015] using a backstripping procedure in the Armorican Massif in France: 50 to 80 m. The latter values seem relatively robust. They confirm previous estimates of 15–50 m (from Jordan, *Turner et al.* [2012]) and are in the same order of magnitude as the eustatic variations documented by *Haq and Schutter* [2008] during the same period of time, though somewhat smaller than the value ~150 m recently reported by *Rasmussen et al.* [2016] based on facies analysis of outcrop sections from Baltica. These discrepancies, i.e., our simulated land ice volume that is too high relative to the geological data, even when considering a slippery bed for the ice sheet (see section 3.3.2), are probably best explained by a significant overestimation of the modeled ice sheet extent. Studies on the last glaciation provide interesting insights into this issue. During the LGM, the Laurentide ice sheet suddenly extended to 40°N [*Ehlers and Gibbard*, 2007], similarly to the Gondwana ice sheet during the first step of Ordovician ice sheet growth. Simultaneously, an ice sheet developed in northern Europe. Northern Asia, on the other side, mysteriously remained ice free at the same latitudes. *Krinner et al.* [2006] suggested that high deposition rates of mineral dust in Asia, due to climate aridity under glacial conditions combined with the proximity to dust sources such as the Gobi desert, prohibited any perennial land ice cover over almost the entire Asian continent during the LGM. The deposition of dust may have similarly restricted the extension of the ice sheet over some regions of Gondwana. An additional cause for the overestimation may be found in our simplified modeling procedure, which imposes a steady pCO_2 forcing until ice sheet-climate equilibrium is reached. *Heinemann et al.* [2014] forced a coupled climate-ice sheet model with realistic orbital and greenhouse gas variations to simulate the Earth system evolution from 78 ka to 0 ka. They successfully simulated, in their transient runs, the Laurentide and Fennoscandian ice sheets evolution over this period of time and also the land ice extent that typifies the LGM. They subsequently ran a simulation by maintaining the LGM orbital configuration and pCO_2 for 90 kyr in order to reach climate-ice sheet equilibrium. Under these conditions, ice sheets extended down to the midlatitudes over both North America and the Eurasian continent, where it was previously restricted to Scandinavia. In the same way, it is reasonable to suppose that the Darriwilian ice sheet never reached full equilibrium due to orbital and/or pCO_2 variations. Such a smaller pre-Hirnantian ice sheet would be consistent with all the existing geological data. It is noteworthy that similar caveats were also suggested by *Horton et al.* [2007] in their simulation of the Late Paleozoic Ice Age. Last but not the least, strong uncertainties remain in paleogeographical and paleoenvironmental reconstructions in deep time [e.g., *Lees et al.*, 2002], and the base maps used in this study might, for instance, overestimate the continental surface situated between the South Pole and 45°S. This would lead to an overestimation of the area available for ice sheet growth and thus of the extent of the ice sheet developing over these latitudes.

4.5. Challenges

Modeling climate and land ice during the early Paleozoic involves numerous processes, which are sometimes difficult to constrain.

Recent studies demonstrated that orbital [*Ghienne et al.*, 2014] and greenhouse gas concentration [*Young et al.*, 2010] variations drove Late Ordovician ice sheet waxing and waning and also Middle Ordovician glacial inceptions [*Turner et al.*, 2012; *Dabard et al.*, 2015]. These phenomena have been shown to control Pleistocene glacial cycles as well [e.g., *Paillard*, 1998], but they cannot yet be precisely reconstructed for the Ordovician (e.g., *Laskar et al.* [2004] for orbital variations). Lack of constraints on these critical boundary conditions has been demonstrated (in the previous section) to significantly impact simulated ice sheet extent during the Middle Ordovician Darriwilian. This also prevents us to capture the high-frequency glacioeustatic variations recently reported in the Middle [*Turner et al.*, 2012; *Dabard et al.*, 2015] and Late [*Ghienne et al.*, 2014] Ordovician. In addition, the simulated ice sheet shows very little sensitivity to orbital and atmospheric forcing once it gets relatively large (Figure 1). Such a behavior was also demonstrated by *Herrmann et al.* [2003] during the Ordovician—although in a lesser extent due to the smaller land ice volume in play in their study—and by *Horton and Poulsen* [2009] in a study about the Late Paleozoic Ice Age. More generally, this strong hysteresis is a major issue in coupled ice sheet-climate studies [e.g., *Huybrechts*, 1993; *Pollard and DeConto*, 2005]. Numerous studies suggest that current ice sheet models may not be sensitive enough to correctly respond to climatic forcing. Melting Last Glacial Maximum ice sheets, for instance, sometimes requires

ad hoc processes, such as input of mineral dust [*Peltier and Marshall*, 1995; *Bonelli et al.*, 2009] or tuning of the PDD coefficients [*Charbit et al.*, 2013]. *Ganopolski et al.* [2010] and *Robinson and Goelzer* [2014] further demonstrated a significant contribution of insolation in surface melt processes, suggesting that the usual PDD melt scheme may constitute a major limitation to simulate the waning of paleo ice sheets. Moreover, recent studies suggest that critical mechanisms may be missing in the building of current ice sheet models, preventing them to simulate correctly the response of land ice to climate changes. The studies recently published by *Pollard et al.* [2015] and *Gasson et al.* [2016], in particular, show that supplementary ice sheet instability mechanisms, such as ice cliff failure and hydrofracturing, are required to correctly simulate the periodic melting of the East and West Antarctic ice sheets during the last ~25 million years. *Austermann et al.* [2015] even suggest that vertical deflections of the continental crust by mantle convective flow, i.e., dynamic topography, may have played a significant role in the Antarctic ice sheet fluctuations during the mid-Pliocene (~3 Ma). *Horton et al.* [2010], in a study about the Late Paleozoic Ice Age, demonstrate that the simulation of glacial-interglacial fluctuations is possible only when they include terrestrial vegetation feedbacks from high-latitude ecosystem changes. They show that changes in vegetation cover amplify the orbitally driven temperature variations. The latter mechanism, however, is not tenable in the Ordovician, when only lichens and mosses covered the land surface [*Steemans et al.*, 2009; *Rubinstein et al.*, 2010].

Beyond the difficulties to simulate the high-frequency temporal evolution of land ice, caveats in modeling the whole deep-time Earth system may induce important errors in continental ice cover numerical reconstruction. Our setup, in particular, does not account for the eustatic sea level fall associated with the growing Gondwana ice sheet, which requires up-to-date bathymetric reconstructions allowing to flood continental areas according to eustatic variations. Such reconstructions exist today [e.g., *Vérard et al.*, 2015], but generally, they are not publicly available.

In summary, the up-to-date deep-time Earth system model employed in this study constitutes an important step forward in modeling Paleozoic climate and ice sheets. Our models notably provide relatively reliable first-order estimates of the temporal and spatial distribution of Ordovician land ice. Uncertainties in the boundary conditions, along with caveats in current ice sheet models, however, prohibit numerical investigation of the high-resolution patterns recently reported based on the Ordovician sedimentary record.

5. Conclusions

In this study, we employed a pioneering deep-time Earth system model to investigate the mechanisms driving Middle to Late Ordovician ice sheet growth, along with the equilibrium ice sheet extent and geometry. Using methods more advanced than earlier reconstructions, our model accounts for ice sheet feedback processes and for orbital variations at the Ordovician obliquity frequency (30 kyr). It was run across the wide spectrum of suggested Ordovician pCO_2 values, 24–3 PAL, resulting in the first simulation portraying the detailed evolution of Middle to Late Ordovician ice sheet growth. Forcing the well-established Ordovician cooling trend with decreasing pCO_2, the emergence of the ice sheet occurs in two steps. In a counterintuitive sequence of events, the vast continental ice sheet appears first and suddenly, covering Gondwana from the South Pole to the midpaleolatitudes. Only during the second act, temperatures drop steeply and sea ice extends. Our models therefore suggest that a single ice sheet extended from the South Pole (North Africa) to the tropics (South Africa) during the latest Ordovician. Scenarios with individual, separate ice centers are not stable and are rejected.

In spite of the particular Ordovician continental configuration potentially inducing a strong continentality over the South Pole, land ice growth is controlled by ablation rather than accumulation. Lack of constraints on Gondwana-wide surface lithology patterns and sediment cover leads to significant uncertainties in modeled land ice volumes. Sensitivity tests demonstrate that the simulated ice sheet spatial extent, however, is reliable and overly dependent neither on the topographic reconstruction nor on the basal dragging parameterization in use.

The sequence of events that we model indicates that glacial onset predated Late Ordovician climate cooling. The comparison with abundant sedimentological, geochemical, and micropaleontological data suggests that the first step in ice sheet growth possibly occurred as early as the Middle Ordovician Darriwilian, in agreement with recent studies reporting third-order eustatic cycles during the same period. Orbital and greenhouse gas variations would have prohibited the ice sheet from reaching long-term equilibrium at this time, explaining the moderate amplitude of reported glacioeustatic variations. The second step in ice sheet growth

is typified by an abrupt global climate cooling by ~14°C, leading to the further extension of the ice sheet into the tropical realm (30°S) during the Hirnantian glacial maximum. By demonstrating that the onset of a pre-Hirnantian continental-scale ice sheet over Gondwana requires no sudden climate cooling, our modeling results supply physical mechanisms for the previously enigmatic Late Ordovician stepped clumped-isotope data, which first display changes in ice volume and only later a drop in tropical sea surface temperatures. Our findings eventually support recent visions of a land ice cover over the supercontinent Gondwana throughout most of the Middle and Late Ordovician, embracing the emerging paradigm of an "Early Paleozoic Ice Age".

This study constitutes a major increment over previously published work that did not account for ice sheet feedback processes. Still, major shortcomings inherent to deep-time studies prevent us from capturing the high-frequency waxing and waning of the ice sheet. Better constrained Ordovician boundary conditions and extensive advances in modeling the cryosphere now constitute a prerequisite for further investigation.

Acknowledgments
We thank David Pollard and an anonymous reviewer for careful and helpful reviews and Heiko Pälike for editorial handling. A.P. also thanks J.-F. Buoncristiani for fruitful discussions and valuable inputs. This work was granted access to the HPC resources of TGCC under the allocation 2014-012212 made by GENCI. T.R.A.V. acknowledges ANR support through grant ANR-12-BS06-0014-SeqStrat-Ice. This research was funded by a CEA PhD grant CFR. This is a contribution to IGCP 591. The code of the FOAM model is available here http://www.mcs.anl.gov/research/projects/foam/index.html. LMDZ can be downloaded from the dedicated website as well http://lmdz.lmd.jussieu.fr/utilisateurs/distribution-du-modele. The code of the GRISLI model is available on request to Catherine Ritz (LGGE, Grenoble). Requests for the model output can be sent to A.P. (alexandre.pohl@lsce.ipsl.fr) or Y.D. (yannick.donnadieu@lsce.ipsl.fr).

References

Alvarez-Solas, J., M. Montoya, C. Ritz, G. Ramstein, S. Charbit, C. Dumas, K. Nisancioglu, T. Dokken, and A. Ganopolski (2011), Heinrich event 1: An example of dynamical ice-sheet reaction to oceanic changes, *Clim. Past*, *7*(4), 1297–1306.

Alvarez-Solas, J., A. Robinson, M. Montoya, and C. Ritz (2013), Iceberg discharges of the last glacial period driven by oceanic circulation changes, *Proc. Natl. Acad. Sci. U.S.A.*, *110*(41), 16350–16354.

Amberg, C. E. A., T. Collart, W. Salenbien, L. M. Egger, A. Munnecke, A. T. Nielsen, C. Monnet, Ø. Hammer, and T. R. A. Vandenbroucke (2016), The nature of Ordovician limestone-marl alternations in the Oslo-Asker District (Norway): Witnesses of primary glacio-eustasy or diagenetic rhythms?, *Sci. Rep.*, *6*, 18787.

Austermann, J., D. Pollard, J. X. Mitrovica, R. Moucha, A. M. Forte, R. M. DeConto, D. B. Rowley, and M. E. Raymo (2015), The impact of dynamic topography change on Antarctic ice sheet stability during the mid-Pliocene warm period, *Geology*, *43*(10), 927–930.

Bennett, M. R. (2003), Ice streams as the arteries of an ice sheet: Their mechanics, stability and significance, *Earth-Sci. Rev.*, *61*(3–4), 309–339.

Berner, R. A. (1990), Atmospheric carbon dioxide levels over Phanerozoic time, *Science*, *249*(4975), 1382–1386.

Berner, R. A. (2006), GEOCARBSULF: A combined model for Phanerozoic atmospheric O_2 and CO_2, *Geochim. Cosmochim. Acta*, *70*(23), 5653–5664.

Blakey, R. C. (2016), Colorado Plateau Geosystems. [Available at http://cpgeosystems.com.]

Bonelli, S., S. Charbit, M. Kageyama, M. N. Woillez, G. Ramstein, C. Dumas, and A. Quiquet (2009), Investigating the evolution of major Northern Hemisphere ice sheets during the last glacial-interglacial cycle, *Clim. Past*, *5*(3), 329–345.

Brenchley, P. J., J. D. Marshall, G. Carden, D. Robertson, D. Long, T. Meidla, L. Hints, and T. F. Anderson (1994), Bathymetric and isotopic evidence for a short-lived Late Ordovician glaciation in a greenhouse period, *Geology*, *22*(4), 295–298.

Bueler, E., and J. Brown (2009), Shallow shelf approximation as a "sliding law" in a thermomechanically coupled ice sheet model, *J. Geophys. Res.*, *114*, F03008, doi:10.1029/2008JF001179.

Buggisch, W., M. M. Joachimski, O. Lehnert, S. M. Bergström, J. E. Repetski, and G. F. Webers (2010), Did intense volcanism trigger the first Late Ordovician icehouse?, *Geology*, *38*(4), 327–330.

Charbit, S., C. Dumas, M. Kageyama, D. M. Roche, and C. Ritz (2013), Influence of ablation-related processes in the build-up of simulated Northern Hemisphere ice sheets during the last glacial cycle, *Cryosphere*, *7*(2), 681–698.

Clark, P. U., and D. Pollard (1998), Origin of the middle Pleistocene transition by ice sheet erosion of regolith, *Paleoceanography*, *13*(1), 1–9.

Crowley, T. J., and S. K. Baum (1991), Toward reconciliation of Late Ordovician (~440 Ma) glaciation with very high CO_2 levels, *J. Geophys. Res.*, *96*(D12), 22,597–22,610.

Crowley, T. J., and S. K. Baum (1995), Reconciling Late Ordovician (440 Ma) glaciation with very high (14X) CO_2 levels, *J. Geophys. Res.*, *100*(D1), 1093–1101.

Dabard, M. P., A. Loi, F. Paris, J.-F. Ghienne, M. Pistis, and M. Vidal (2015), Sea-level curve for the Middle to early Late Ordovician in the Armorican Massif (western France): Icehouse third-order glacio-eustatic cycles, *Palaeogeogr. Palaeoclimatol. Palaeoecol.*, *436*, 96–111.

DeConto, R. M., and D. Pollard (2003), Rapid Cenozoic glaciation of Antarctica induced by declining atmospheric CO_2, *Nature*, *421*(6920), 245–249.

Denis, M., J.-F. Buoncristiani, M. Konaté, J.-F. Ghienne, and M. Guiraud (2007), Hirnantian glacial and deglacial record in SW Djado Basin (NE Niger), *Geodin. Acta*, *20*(3), 177–195.

Denis, M., M. Guiraud, M. Konaté, and J. F. Buoncristiani (2010), Subglacial deformation and water-pressure cycles as a key for understanding ice stream dynamics: Evidence from the Late Ordovician succession of the Djado Basin (Niger), *Int. J. Earth Sci.*, *99*(6), 1399–1425.

Díaz-Martínez, E., and Y. Grahn (2007), Early Silurian glaciation along the western margin of Gondwana (Peru, Bolivia and northern Argentina): Palaeogeographic and geodynamic setting, *Palaeogeogr. Palaeoclimatol. Palaeoecol.*, *245*(1), 62–81.

Ehlers, J., and P. L. Gibbard (2007), The extent and chronology of Cenozoic global glaciation, *Quat. Int.*, *164–165*, 6–20.

Elrick, M., D. Reardon, W. Labor, J. Martin, A. Desrochers, and M. Pope (2013), Orbital-scale climate change and glacioeustasy during the early Late Ordovician (pre-Hirnantian) determined from $\delta^{18}O$ values in marine apatite, *Geology*, *41*(7), 775–778.

Finnegan, S., K. Bergmann, J. M. Eiler, D. S. Jones, D. A. Fike, I. Eisenman, N. C. Hughes, A. K. Tripati, and W. W. Fischer (2011), The magnitude and duration of Late Ordovician-Early Silurian glaciation, *Science*, *331*(6019), 903–906.

François, L., A. Grard, and Y. Goddéris (2005), Modelling atmospheric CO_2 changes at geological time scales, in *Pre-Cambrian to Palaeozoic Palaeopalynology and Palaeobotany*, edited by P. Steemans and E. Javaux, Carnets de Géologie/Notebooks on Geology, Memoir 2005/02, Brest, France.

Fretwell, P., et al. (2013), Bedmap2: Improved ice bed, surface and thickness datasets for Antarctica, *Cryosphere*, *7*(1), 375–393.

Ganopolski, A., R. Calov, and M. Claussen (2010), Simulation of the last glacial cycle with a coupled climate ice-sheet model of intermediate complexity, *Clim. Past*, *6*, 229–244.

Gasson, E., R. M. DeConto, D. Pollard, and R. H. Levy (2016), Dynamic Antarctic ice sheet during the early to mid-Miocene, *Proc. Natl. Acad. Sci. U.S.A.*, *113*(13), 3459–3464, doi:10.1073/pnas.1516130113.

Ghienne, J.-F., D. P. Le Heron, J. Moreau, M. Denis, and M. Deynoux (2007), The Late Ordovician glacial sedimentary system of the North Gondwana platform, in *Glacial Sedimentary Processes and Products, Spec. Publ. Int. Assoc. of Sedimentologists*, edited by M. Hambrey et al., pp. 295–319, Blackwells, Oxford, U. K.

Ghienne, J.-F., et al. (2014), A Cenozoic-style scenario for the end-Ordovician glaciation, *Nat. Commun.*, *5*, 4485.
Goddéris, Y., Y. Donnadieu, G. Le Hir, V. Lefebvre, and E. Nardin (2014), The role of palaeogeography in the Phanerozoic history of atmospheric CO_2 and climate, *Earth Sci. Rev.*, *128*, 122–138.
Gough, D. O. (1981), Solar interior structure and luminosity variations, *Sol. Phys.*, *74*, 21–34.
Haq, B. U., and S. R. Schutter (2008), A chronology of paleozoic sea-level changes, *Science*, *322*(5898), 64–68.
Heimbach, P., and M. Losch (2012), Adjoint sensitivities of sub-ice-shelf melt rates to ocean circulation under the Pine Island Ice Shelf, West Antarctica, *Ann. Glaciol.*, *53*(60), 59–69.
Heinemann, M., A. Timmermann, O. Elison Timm, F. Saito, and A. Abe-Ouchi (2014), Deglacial ice sheet meltdown: Orbital pacemaking and CO_2 effects, *Clim. Past*, *10*(4), 1567–579.
Herrmann, A. D., M. E. Patzkowsky, and D. Pollard (2003), Obliquity forcing with 8–12 times preindustrial levels of atmospheric pCO_2 during the Late Ordovician glaciation, *Geology*, *31*(6), 485–488.
Herrmann, A. D., M. E. Patzkowsky, and D. Pollard (2004), The impact of paleogeography, pCO_2, poleward ocean heat transport and sea level change on global cooling during the Late Ordovician, *Palaeogeogr. Palaeoclimatol. Palaeoecol.*, *206*(1), 59–74.
Horton, D. E., and C. J. Poulsen (2009), Paradox of late Paleozoic glacioeustasy, *Geology*, *37*(8), 715–718.
Horton, D. E., C. J. Poulsen, and D. Pollard (2007), Orbital and CO_2 forcing of late Paleozoic continental ice sheets, *Geophys. Res. Lett.*, *34*, L19708, doi:10.1029/2007GL031188.
Horton, D. E., C. J. Poulsen, and D. Pollard (2010), Influence of high-latitude vegetation feedbacks on late Palaeozoic glacial cycles, *Nat. Geosci.*, *3*(8), 572–577.
Hourdin, F., et al. (2013), Impact of the LMDZ atmospheric grid configuration on the climate and sensitivity of the IPSL-CM5A coupled model, *Clim. Dyn.*, *40*, 2167–2192.
Huybrechts, P. (1993), Glaciological modelling of the Late Cenozoic East Antarctic ice sheet: Stability or dynamism?, *Geogr. Ann.*, *75*(A), 221–238.
Jacob, R. L. (1997), Low frequency variability in a simulated atmosphere ocean system, PhD thesis, Univ. of Wisconsin-Madison, Madison, Wisconsin.
Krinner, G., O. Boucher, and Y. Balkanski (2006), Ice-free glacial northern Asia due to dust deposition on snow, *Clim. Dyn.*, *27*(6), 613–625.
Ladant, J. B., Y. Donnadieu, V. Lefebvre, and C. Dumas (2014), The respective role of atmospheric carbon dioxide and orbital parameters on ice sheet evolution at the Eocene-Oligocene transition, *Paleoceanography*, *29*, 810–823, doi:10.1002/2013PA002593.
Laskar, J., P. Robutel, F. Joutel, M. Gastineau, A. Correia, and B. Levrard (2004), A long-term numerical solution for the insolation quantities of the Earth, *Astron. Astrophys.*, *428*(1), 261–285.
Le Heron, D. P., and J. A. Dowdeswell (2009), Calculating ice volumes and ice flux to constrain the dimensions of a 440 Ma North African ice sheet, *J. Geol. Soc.*, *166*(2), 277–281.
Le Heron, D. P., J.-F. Ghienne, M. El Houicha, Y. Khoukhi, and J.-L. Rubino (2007), Maximum extent of ice sheets in Morocco during the Late Ordovician glaciation, *Palaeogeogr. Palaeoclimatol. Palaeoecol.*, *245*(1–2), 200–226.
Lees, D. C., R. A. Fortey, and L. R. M. Cocks (2002), Quantifying paleogeography using biogeography: A test case for the Ordovician and Silurian of Avalonia based on brachiopods and trilobites, *Paleobiology*, *28*(3), 343–363.
Licht, A., et al. (2014), Asian monsoons in a late Eocene greenhouse world, *Nature*, *513*(7519), 501–506.
Lowry, D. P., C. J. Poulsen, D. E. Horton, T. H. Torsvik, and D. Pollard (2014), Thresholds for Paleozoic ice sheet initiation, *Geology*, *42*(7), 627–630.
Loi, A., et al. (2010), The Late Ordovician glacio-eustatic record from a high-latitude storm-dominated shelf succession: The Bou Ingarf section (Anti-Atlas, Southern Morocco), *Palaeogeogr. Palaeoclimatol. Palaeoecol.*, *296*(3–4), 332–358.
Moreau, J., J.-F. Ghienne, D. P. L. Heron, J.-L. Rubino, and M. Deynoux (2005), 440 Ma ice stream in North Africa, *Geology*, *33*(9), 753–756.
Nardin, E., Y. Goddéris, Y. Donnadieu, G. Le Hir, R. C. Blakey, E. Pucéat, and M. Aretz (2011), Modeling the early Paleozoic long-term climatic trend, *Geol. Soc. Am. Bull.*, *123*(5–6), 1181–1192.
Nielsen, A. T. (2004), Ordovician sea-level changes: A Baltoscandian perspective, in *The Great Ordovician Biodiversification Event*, edited by B. D. Webby et al., pp. 84–93, Columbia Univ. Press, New York.
Page, A., J. A. Zalasiewicz, M. Williams, and L. E. Popov (2007), Were transgressive black shales a negative feedback modulating glacioeustasy in the Early Palaeozoic Icehouse?, in *Deep-Time Perspectives on Climate Change: Marrying the Signal from Computer Models and Biological Proxies*, edited by M. Williams et al., pp. 123–156, The Micropalaeontological Soc., Spec. Publ., The Geolog. Soc., London, U. K.
Paillard, D. (1998), The timing of Pleistocene glaciations from a simple multiple-state climate model, *Nature*, *391*, 378–381.
Pancost, R. D., K. H. Freeman, A. D. Herrmann, M. E. Patzkowsky, L. Ainsaar, and T. Martma (2013), Reconstructing Late Ordovician carbon cycle variations, *Geochim. Cosmochim. Acta*, *105*, 433–454.
Peltier, W. R., and S. Marshall (1995), Coupled energy-balance/ice-sheet model simulations of the glacial cycle: A possible connection between terminations and terrigenous dust, *J. Geophys. Res.*, *100*(D7), 14,269–14,289.
Peyaud, V., C. Ritz, and G. Krinner (2007), Modelling the Early Weichselian Eurasian Ice Sheets: Role of ice shelves and influence of ice-dammed lakes, *Clim. Past*, *3*, 375–386.
Pohl, A., Y. Donnadieu, G. Le Hir, J. F. Buoncristiani, and E. Vennin (2014), Effect of the Ordovician paleogeography on the (in)stability of the climate, *Clim. Past*, *10*(6), 2053–2066.
Pohl, A., E. Nardin, T. Vandenbroucke, and Y. Donnadieu (2015), High dependence of Ordovician ocean surface circulation on atmospheric CO_2 levels, *Palaeogeogr. Palaeoclimatol. Palaeoecol.*, doi:10.1016/j.palaeo.2015.09.036, in press.
Pollard, D. (2010), A retrospective look at coupled ice sheet-climate modeling, *Clim. Change*, *100*(1), 173–194.
Pollard, D., and R. M. DeConto (2005), Hysteresis in Cenozoic Antarctic ice-sheet variations, *Global Planet. Change*, *45*(1–3), 9–21.
Pollard, D., and R. M. DeConto (2012), Description of a hybrid ice sheet-shelf model, and application to Antarctica, *Geosci. Model Dev.*, *5*, 1273–1275.
Pollard, D., R. M. DeConto, and R. B. Alley (2015), Potential Antarctic Ice Sheet retreat driven by hydrofracturing and ice cliff failure, *Earth Planet. Sci. Lett.*, *412*, 112–121.
Quiquet, A., C. Ritz, H. J. Punge, and D. Salas y Mélia (2013), Greenland ice sheet contribution to sea level rise during the last interglacial period: A modelling study driven and constrained by ice core data, *Clim. Past*, *9*(1), 353–366.
Rasmussen, C. M. Ø., et al. (2016), Onset of main Phanerozoic marine radiation sparked by emerging Mid Ordovician icehouse, *Sci. Rep.*, *6*, 18884.
Ravier, E., J. F. Buoncristiani, J. Menzies, M. Guiraud, S. Clerc, and E. Portier (2015), Does porewater or meltwater control tunnel valley genesis? Case studies from the Hirnantian of Morocco, *Palaeogeogr. Palaeoclimatol. Palaeoecol.*, *418*, 359–376.
Raymo, M. E., J. X. Mitrovica, M. J. O'Leary, R. M. DeConto, and P. J. Hearty (2011), Departures from eustasy in Pliocene sea-level records, *Nat. Geosci.*, *4*(5), 328–332.

Reeh, N. (1991), Parameterization of melt rate and surface temperature on the Greenland ice sheet, *Polarforschung*, *59*(1), 113–128.
Ritz, C., V. Rommelaere, and C. Dumas (2001), Modeling the evolution of Antarctic ice sheet over the last 420,000 years—Implications for altitude changes in the Vostok region, *J. Geophys. Res.*, *106*(D23), 31,943–31,964.
Robinson, A., and H. Goelzer (2014), The importance of insolation changes for paleo ice sheet modeling, *Cryosphere*, *8*(4), 1419–1428.
Rothman, D. H. (2002), Atmospheric carbon dioxide levels for the last 500 million years, *Proc. Natl. Acad. Sci. U.S.A.*, *99*(7), 4167–4171.
Rubinstein, C. V., P. Gerrienne, G. S. de la Puente, R. A. Astini, and P. Steemans (2010), Early Middle Ordovician evidence for land plants in Argentina (eastern Gondwana), *New Phytol.*, *188*(2), 365–369.
Scotese, C. R. (2016), PALEOMAP Project. [Availble at http://www.scotese.com.]
Scotese, C. R., and W. S. McKerrow (1991), Ordovician plate tectonic reconstructions, in *Advances in Ordovician Geology*, edited by C. R. Scotese and W. S. McKerrow, pp. 271–282, Geol. Surv. of Canada, Ottawa, Ontario.
Semtner, A. J. (1976), A model for the thermodynamic growth of sea ice in numerical investigations of climate, *J. Phys. Oceanogr.*, *6*(3), 379–389.
Sheehan, P. M. (2001), The late Ordovician mass extinction, *Annu. Rev. Earth Planet. Sci.*, *29*(1), 331–364.
Steemans, P., A. Le Herissé, J. Melvin, M. A. Miller, F. Paris, J. Verniers, and C. H. Wellman (2009), Origin and radiation of the earliest vascular land plants, *Science*, *324*(5925), 353–353.
Stocchi, P., C. Escutia, A. J. P. Houben, B. L. A. Vermeersen, P. K. Bijl, H. Brinkhuis, R. M. DeConto, S. Galeotti, S. Passchier, and D. Pollard (2013), Relative sea-level rise around East Antarctica during Oligocene glaciation, *Nat. Geosci.*, *6*(5), 380–384.
Tabor, C. R., and C. J. Poulsen (2016), Simulating the mid-Pleistocene transition through regolith removal, *Earth Planet. Sci. Lett.*, *434*(C), 231–240.
Tobin, K. J., and S. M. Bergström (2002), Implications of Ordovician (460 Myr) marine cement for constraining seawater temperature and atmospheric pCO_2, *Palaeogeogr. Palaeoclimatol. Palaeoecol.*, *181*(4), 399–417.
Tobin, K. J., S. M. Bergström, and P. De La Garza (2005), A mid-Caradocian (453 Ma) drawdown in atmospheric pCO_2 without ice sheet development?, *Palaeogeogr. Palaeoclimatol. Palaeoecol.*, *226*(3–4), 187–204.
Torsvik, T. H., and L. R. M. Cocks (2009), BugPlates: Linking biogeography and palaeogeography, software manual. [Available at http://www.geodynamics.no.]
Torsvik, T. H., and L. R. M. Cocks (2013), New global palaeogeographical reconstructions for the Early Palaeozoic and their generation, in *Early Palaeozoic Biogeography and Palaeogeography, Geol. Soc. of London Memoirs*, edited by D. A. T. Harper and T. Servais, pp. 5–24, The Geol. Soc., London, U. K.
Trotter, J. A., I. S. Williams, C. R. Barnes, C. Lécuyer, and R. S. Nicoll (2008), Did cooling oceans trigger Ordovician biodiversification? Evidence from conodont thermometry, *Science*, *321*, 550–554.
Turner, B. R., H. A. Armstrong, C. R. Wilson, and I. M. Makhlouf (2012), High frequency eustatic sea-level changes during the Middle to early Late Ordovician of southern Jordan: Indirect evidence for a Darriwilian Ice Age in Gondwana, *Sediment. Geol.*, *251*, 34–48.
Vandenbroucke, T. R. A., H. A. Armstrong, M. Williams, J. A. Zalasiewicz, and K. Sabbe (2009), Ground-truthing Late Ordovician climate models using the paleobiogeography of graptolites, *Paleoceanography*, *24*, PA4202, doi:10.1029/2008PA001720.
Vandenbroucke, T. R. A., H. A. Armstrong, M. Williams, F. Paris, J. A. Zalasiewicz, K. Sabbe, J. Nølvak, T. J. Challands, J. Verniers, and T. Servais (2010a), Polar front shift and atmospheric CO_2 during the glacial maximum of the Early Paleozoic Icehouse, *Proc. Natl. Acad. Sci. U.S.A.*, *107*(34), 14,983–14,986.
Vandenbroucke, T. R. A., H. A. Armstrong, M. Williams, F. Paris, K. Sabbe, J. A. Zalasiewicz, J. Nølvak, and J. Verniers (2010b), Epipelagic chitinozoan biotopes map a steep latitudinal temperature gradient for earliest Late Ordovician seas: Implications for a cooling Late Ordovician climate, *Palaeogeogr. Palaeoclimatol. Palaeoecol.*, *294*(3–4), 202–219.
Vérard, C., C. Hochard, P. O. Baumgartner, G. M. Stampfli, and M. Liu (2015), 3D palaeogeographic reconstructions of the Phanerozoic versus sea, *J. Palaeogeogr.*, *4*(1), 64–84.
Wenzel, B., C. Lécuyer, and M. M. Joachimski (2000), Comparing oxygen isotope records of Silurian calcite and phosphate—$\delta^{18}O$ compositions of brachiopods and conodonts, *Geochim. Cosmochim. Acta*, *64*(11), 1859–1872.
Williams, G. E. (1991), Milankovitch-band cyclicity in bedded halite deposits contemporaneous with Late Ordovician-Early Silurian glaciation, Canning Basin, Western Australia, *Earth Planet. Sci. Lett.*, *103*(1), 143–155.
Yapp, C. J., and H. Poths (1992), Ancient atmospheric CO_2 pressures inferred from natural goethites, *Nature*, *355*, 342–344.
Yapp, C. J., and H. Poths (1996), Carbon isotopes in continental weathering environments and variations in ancient atmospheric CO_2 pressure, *Earth Planet. Sci. Lett.*, *137*(1), 71–82.
Young, S. A., M. R. Saltzman, K. A. Foland, J. S. Linder, and L. R. Kump (2009), A major drop in seawater $^{87}Sr/^{86}Sr$ during the Middle Ordovician (Darriwilian): Links to volcanism and climate?, *Geology*, *37*(10), 951–954.
Young, S. A., M. R. Saltzman, W. I. Ausich, A. Desrochers, and D. Kaljo (2010), Did changes in atmospheric CO_2 coincide with latest Ordovician glacial–interglacial cycles?, *Palaeogeogr. Palaeoclimatol. Palaeoecol.*, *296*(3–4), 376–388.